



NASA CR-159336

# NASA Contractor Report 159336

NASA-CR-159336

1981 0010904

## An Investigation of Self-Subtraction Holography in LiNbO<sub>3</sub>

**D. W. Vahey, R. P. Kenan,  
N. F. Hartman, and R. C. Sherman**

**Battelle Columbus Laboratories  
505 King Avenue  
Columbus, Ohio 43201**

**Contract NAS1-15736  
March, 1981**



National Aeronautics and  
Space Administration

**Langley Research Center  
Hampton, Virginia 23665**



NF01163

LIBRARY COPY

APR 8 1981

LANGLEY RESEARCH CENTER  
HAMPTON, VIRGINIA

NASA Contractor Report 159336

# An Investigation of Self-Subtraction Holography in $\text{LiNbO}_3$

D. W. Vahey, R. P. Kenan,  
N. F. Hartman, and R. C. Sherman

Battelle Columbus Laboratories  
505 King Avenue  
Columbus, Ohio 43201

Contract NAS1-15736  
March, 1981

The NASA logo, consisting of the word "NASA" in a bold, sans-serif font.

National Aeronautics and  
Space Administration

**Langley Research Center**  
Hampton, Virginia 23665

N81-19431#

**This Page Intentionally Left Blank**

TABLE OF CONTENTS

	<u>Page</u>
SUMMARY. . . . .	1
I. INTRODUCTION . . . . .	3
Definition of Self-Subtraction Holography . . . . .	3
Advantages of Self-Subtraction Holography . . . . .	3
Accomplishments of the Self-Subtraction Program . . . . .	5
II. TECHNICAL BACKGROUND . . . . .	7
A Physical Description of Self-Subtraction. . . . .	7
The Photorefractive Process . . . . .	9
The Origin of Donors and Traps . . . . .	11
The Migration of Photoexcited Electrons. . . . .	11
The Photorefractive Equations. . . . .	13
Theoretical Analysis of Self-Subtraction. . . . .	15
Case I. $Q = 0, R_o = S_o$ . . . . .	20
Case II. $Q = \pi/2, R_o \gg S_o$ . . . . .	21
Case III. The General Case . . . . .	22
Status of the Theoretical Understanding of Hologram Formation in $\text{LiNbO}_3$ . . . . .	29
III. EXPERIMENTAL METHODS FOR THE STUDY OF SELF-SUBTRACTION . . . . .	30
The Use of Optical Waveguide Samples. . . . .	30
The Sample Geometry . . . . .	31
The Arrangement of Experimental Apparatus . . . . .	34
Data Acquisition. . . . .	34
A Phase Tracking Experiment . . . . .	37
Sample Preparation Techniques . . . . .	39
IV. RESULTS OF EXPERIMENTAL STUDIES OF SELF-SUBTRACTION . . . . .	41
Experimental Studies of Self Subtraction in Outdiffused Waveguide Sample #96. . . . .	41
Tests of Sample #96 as a Self-Subtraction Processor. . . . .	42
Time Constants, Contrast Ratios, and Reproducibility of Self Subtraction Holograms. . . . .	42
Sensitivity of Self Subtraction Holograms to Applied Phase Shifts. . . . .	48

TABLE OF CONTENTS  
(Continued)

	<u>Page</u>
Stability of a Self-Subtraction Hologram to Continuous Seven-Hour Readout. . . . .	51
Sensitivity of Self-Subtraction Holography to Bragg Angle. . . . .	54
Sensitivity of Self-Subtraction Holography to Thermal Oxidizing and Reducing Treatments. . .	55
Experimental Studies of Self Subtraction in Outdiffused Waveguide Samples #'s 97, 100, and 162 . . . . .	58
Performance of Sample #97 . . . . .	58
Performance of Sample #100. . . . .	59
Performance of Sample #162. . . . .	61
Experimental Studies of Self-Subtraction in Ti-Indiffused Waveguide Sample #135. . . . .	64
Comparison of Theory and Experiment. . . . .	66
Subtracted-Beam Intensity Versus Time . . . . .	66
Subtracted-Beam Phase Versus Time . . . . .	66
V. SUMMARY AND CONCLUSIONS . . . . .	70
REFERENCES. . . . .	72

LIST OF FIGURES

Figure	I-1. The Holographic Subtraction Process . . . . .	4
Figure	II-1. Interference Pattern and Corresponding Refractive-Index Pattern after Hologram Formation. . . . .	8
Figure	II-2. Interference Pattern and Index Pattern After A $\pi/4$ Phase Shift Applied to the Signal Beam. . . . .	10
Figure	II-3. Conceptual Drawing Showing Redistribution of Filled Traps during Illumination by an Interference Pattern. . . . .	12
Figure	II-4. Signal-Beam Intensity Vs Recording Time . . . . .	23
Figure	II-5. Signal-Beam Intensity Vs Recording Time . . . . .	24
Figure	II-6. Signal-Beam Phase Vs Recording Time for $(S_o/R_o)^2 = 0.01$ and $Q = 1.5$ . . . . .	27
Figure	II-7. Signal-Beam Phase Vs Recording Time for $S_o^2 = R_o^2 = 1/2$ , $Q = 1.4$ . . . . .	28
Figure	III-1. The Sample-Optical Beam Configuration . . . . .	32

LIST OF FIGURES

(Continued)

		<u>Page</u>
Figure III-2.	Experimental Arrangement for Self-Subtraction Studies.	35
Figure III-3.	Experimental Configuration for Tracking the Phase of Signal Beam During Hologram Recording. . . . .	38
Figure IV-1.	Power-Vs-Time for a Subtracted Beam that Experiences a $\pi$ -Phase Shift at $t = 0$ and Writes to a Renewed Condition of Self Subtraction . . . . .	44
Figure IV-2.	Power-Vs-Time for a Subtracted Beam that Experiences a $\pi/4$ Phase Shift at $t = 0$ and Writes to a Renewed Condition of Self Subtraction. . . . .	46
Figure IV-3.	Power-Vs-Time for a Subtracted Beam that Experiences Second $\pi$ Phase Shift and Writes to a Renewed Condition of Self Subtraction. . . . .	47
Figure IV-4.	Intensity Vs Time for a Subtracted Beam in the Presence of Externally Applied Phase Shifts . . . . .	49
Figure IV-5.	Variation of Signal Beam Intensity with Applied Phase Shift. . . . .	50
Figure IV-6.	Power-Vs-Time Characteristics Observed During the First 30 min of a 7 h Stability Test . . . . .	52
Figure IV-7.	Subtracted Power (Vertical) Vs Time (Horizontal) in the Interval 0.5-7.0 h . . . . .	53
Figure IV-8.	Self-Subtraction Characteristics of Holograms in Out-diffused LiNbO <sub>3</sub> Waveguide #96, Measured for Five Different Bragg Angles. . . . .	56
Figure IV-9.	Signal-Beam Intensity Vs Time for Sample #97 Following an Oxidizing Thermal Treatment . . . . .	60
Figure IV-10.	Temporal Variation of Signal and Reference-Beam Intensity in the Presence of Five Applied Phase Shifts. . .	63
Figure IV-11.	Oscillating Output Power for the Weaker of Two Beams Used to Write a Hologram in a Ti:LiNbO <sub>3</sub> Waveguide. . .	65
Figure IV-12.	Damped Oscillatory Signal-Beam Intensity Vs Time Characteristics Exhibited by Sample #162A. . . . .	67
Figure IV-13.	Experimental Determination of Signal-Beam Intensity and Phase Variations During Hologram Recording . . . .	69

AN INVESTIGATION OF SELF-SUBTRACTION  
HOLOGRAPHY IN  $\text{LiNbO}_3$

D. W. Vahey, R. P. Kenan, N. F. Hartman, and R. C. Sherman

Battelle Columbus Laboratories

SUMMARY

This report describes the results of a fifteen-month investigation of self-subtraction holography in  $\text{LiNbO}_3$  optical waveguides. Self subtraction is the term used to describe the gradual transfer of energy from one optical beam to another that can occur when the two beams are used to record a hologram in  $\text{LiNbO}_3$  or other photorefractive materials. The effect is potentially useful in optical processors where the information signal is superimposed on a slowly varying and uninteresting background signal. Self subtraction affords the possibility of eliminating the background from the total signal received.

The quality of self subtraction is inferred from measurements of the time required to form the hologram, the minimum beam intensity generated, the ability of the  $\text{LiNbO}_3$  to form many successive holograms without fatigue, and the stability of the holograms during long-term readout. In this program we tested in depth one sample having self-subtraction characteristics that were very promising: hologram-formation times were on the order of 150 sec, the null signal was less than 2.5% of the peak signal, and no fatigue nor instability was detected over the span of the experiments. Another sample, fabricated similarly or with slight modifications did not perform nearly as well. In all samples, attempts to improve self-subtraction characteristics by various thermal treatments had no effect or had adverse effects, with one exception in which improvement was noted after a time delay of several days.

A theory developed to describe self subtraction showed the observed decrease in beam intensity with time, but the shape of the predicted decay curve was oscillatory in contrast to the exponential-like decay observed. The theory was also inadequate to account for the experimental sensitivity of self subtraction to the Bragg angle of the hologram.

We conclude that self subtraction is a viable method for optical processing systems requiring background discrimination. However, understanding the physical basis for the effect has only begun and further work of both an experimental and theoretical nature is required in order to optimize and control self subtraction for use in applications.

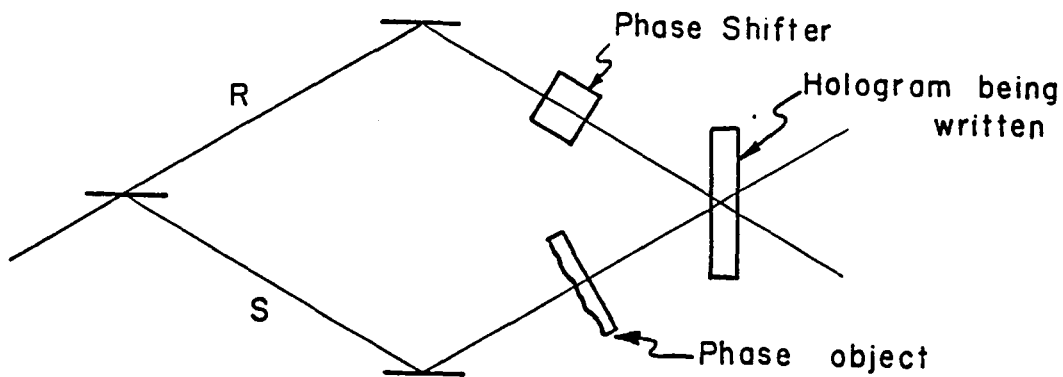
## I. INTRODUCTION

### DEFINITION OF SELF-SUBTRACTION HOLOGRAPHY

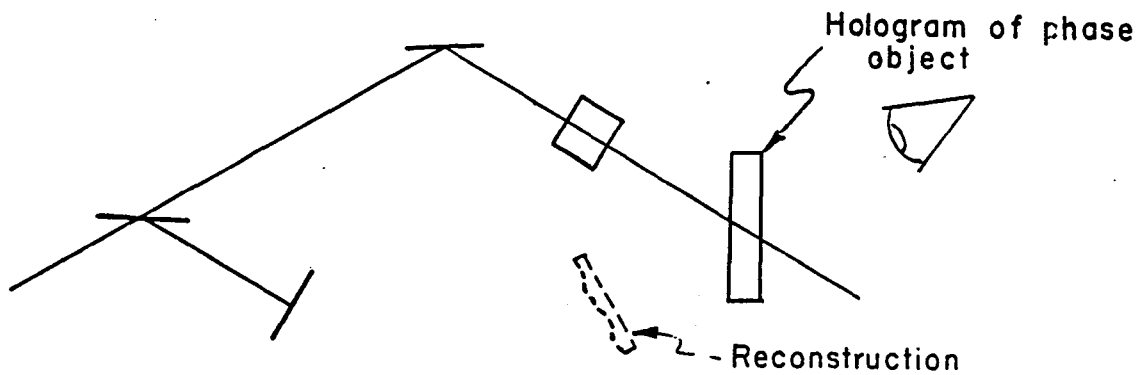
Self-subtraction holography is the process by which one of two beams used to write a hologram gradually transfers its energy to the other beam during hologram formation, and emerges from the hologram region with decreasing intensity. The designation of the term "self-subtraction" to describe this phenomenon is not obvious unless one views it as a special case of the technique known as holographic subtraction. In this technique, shown in Fig. 1, a viewer or other sensing system detects the coherent superposition of two wavefronts. One is the instantaneous wavefront from a specific object that passes through a hologram of that object without being diffracted. The other wavefront is generated by reconstruction in the hologram. If the relative phase of the two wavefronts is adjusted to  $\pi$ , they will destructively interfere and the viewer will see a dark field. It is said that the reconstructed wavefront is subtracted from the real wavefront; hence we have the terminology "holographic subtraction".<sup>(1)</sup> In this example it was implied to be necessary to adjust the relative phase shift between wavefronts to  $\pi$  by an external means, such as a phase shifter. In certain holographic materials, such as  $\text{LiNbO}_3$ , the relative phase between the reconstructed wavefront and the real wavefront is equal or close to  $\pi$  by virtue of the hologram-formation mechanism.<sup>(2)</sup> In this case, an externally applied phase adjustment is not necessary to achieve the subtracted condition. The situation here is therefore called self-subtraction.

### ADVANTAGES OF SELF-SUBTRACTION HOLOGRAPHY

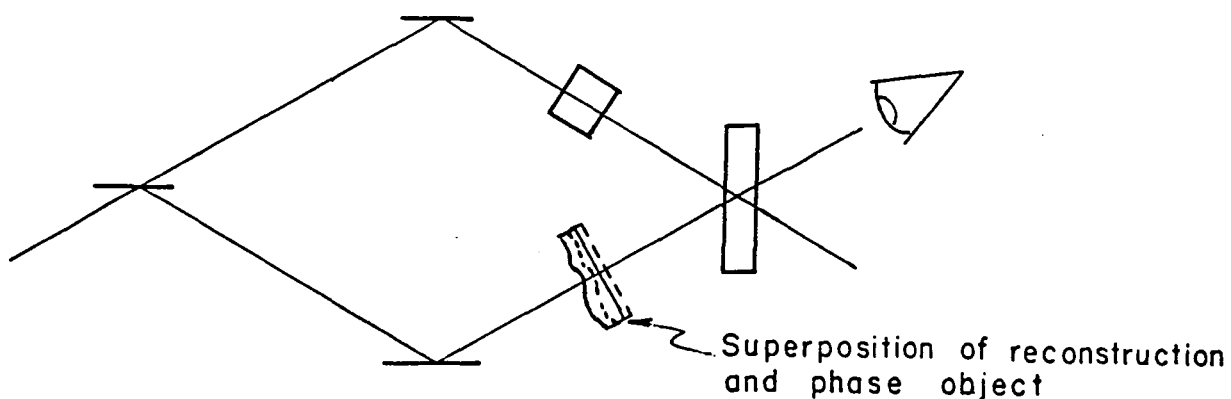
The potential applications for self-subtraction holography are the same as those for subtraction holography in general. By use of this technique, one hopes to more readily detect small changes in objects or scenes under study. A specific application which has been a motivating force for this investigation is that of the Integrated Optical Data Preprocessor,



(a) THE FORMATION OF THE HOLOGRAM OF A PHASE OBJECT



(b) RECONSTRUCTION OF OBJECT WITH SIGNAL BEAM BLOCKED



(c) SUPERPOSITION OF OBJECT AND IMAGE. AN APPROPRIATE PHASE SHIFT WILL RESULT IN THE OBSERVER SEEING A DARK FIELD

FIGURE I-1. THE HOLOGRAPHIC SUBTRACTION PROCESS.

currently under development at Battelle.<sup>(3)</sup> In this application the "object" is a spatial phase modulation imposed on an optical guided wavefront. The phase modulation is achieved by applying voltages from an array of sensors to an array of electrodes spanning a waveguided beam in electrooptic  $\text{LiNbO}_3$ . Changes in the wavefront are detected by holographic subtraction and provide a direct indication of changes in the voltages provided by the sensors. The usual situation is that in which sudden changes in sensor voltages represent phenomena that are of interest, while slow variations reflect changes in the ambient background and are to be ignored. Conventional holographic subtraction, in addition to requiring an externally applied phase shift, uses permanent holograms geared to specific sensor outputs, and so indiscriminately detects both fast and slow changes in these outputs. However, self-subtraction holograms are continuously updated in time, and so detect only those sensor outputs that change more rapidly than the characteristic update time constant, as required.

#### ACCOMPLISHMENTS OF THE SELF-SUBTRACTION PROGRAM

With this system application in mind, it is appropriate to describe the accomplishments of the self-subtraction program. Working with holograms formed in  $\text{LiNbO}_3$  optical waveguides, we performed experiments which served to characterize the phenomenon with regard to (1) the extent to which the subtracted optical beam could be extinguished, (2) the time constants associated with hologram formation, and (3) the material fatigue associated with the continuous updating of the self-subtraction hologram. Our results in the characterization phase were very encouraging, showing 40-to-1 maximum-to-minimum signal ratios, time constants on the order of  $10^2$  sec, hologram stability greater than 7 hours under constant exposure, and hologram recycleability greater than 9 cycles without any signs of degradation.

We also performed experiments designed to elucidate the physical mechanisms for self-subtraction, and to optimize the effect for use in holographic optical-processing systems. These experiments involved the modification of optical beam ratios, beam intensities and beam widths, the use of both Ti-diffused and Li-outdiffused  $\text{LiNbO}_3$  waveguides, the variation of the hologram grating period, and the use of various reducing/oxidizing thermal treatments.

Although a variety of interesting phenomena were observed and a reasonably reproducible procedure was determined for obtaining useful self-subtraction characteristics in  $\text{LiNbO}_3$  waveguides, these experiments were not particularly useful in elucidating the physical mechanisms of self subtraction. A theory was developed based on the simplest physical model that appeared to have the sophistication necessary to describe the basic self-subtraction phenomenon. In so far as it was possible to test the theory during the program, however, the agreement with experiment left something to be desired.

In summary, we were successful in characterizing the phenomena of self subtraction experimentally, and in determining a set of conditions for producing good self subtraction in outdiffused  $\text{LiNbO}_3$  waveguides. The results were encouraging with regard to the eventual use of the phenomenon in practical systems. Yet much work remains to be done to understand the physics of self subtraction and to optimize the effect for use in applications.

## II. TECHNICAL BACKGROUND

In this section we describe our current understanding of the physical basis for self-subtraction holography. First we describe the spatial phase relationship between the index-modulation pattern of a hologram and the interference pattern of the writing beams that leads to subtraction. Then we describe how this spatial relationship may result automatically in the case of photorefractive holographic materials like  $\text{LiNbO}_3$ . Then we develop a more rigorous description of self subtraction based on a common model for photorefractivity, and we indicate some of the behavior predicted by this model. This will lead us naturally into a discussion of our experiments and experimental results in Sec. III.

### A PHYSICAL DESCRIPTION OF SELF-SUBTRACTION

Figure II-1 shows the interference pattern formed by two beams of unit intensity that have combined to form a hologram in a photosensitive material. The drawing indicates schematically that the relative phase between the interference maxima and the refractive index maxima of the hologram is zero; that is, intensity maxima and index maxima overlap. The symmetry of the situation dictates that the output intensities of the two optical beams will each be unity, since they were taken to be unity at the hologram input. In any event, the output beams may be regarded as being composed of diffracted and undiffracted components of the input beams  $R_0$  and  $S_0$ . If  $\eta$  is the diffraction efficiency of the hologram, we may write

$$S = (1-\eta)^{1/2} S_0 + e^{i\psi} (\eta)^{1/2} R_0 \quad (\text{II-1})$$

$$R = (1-\eta)^{1/2} R_0 + e^{i\psi} (\eta)^{1/2} S_0 ,$$

where the first term on the right of each equation is the undiffracted contribution to the output amplitude, and the second is the diffracted contribution. A natural phase shift  $\psi$  has been associated with the diffraction process. The existence of such a phase shift is seen to be imposed by the symmetry

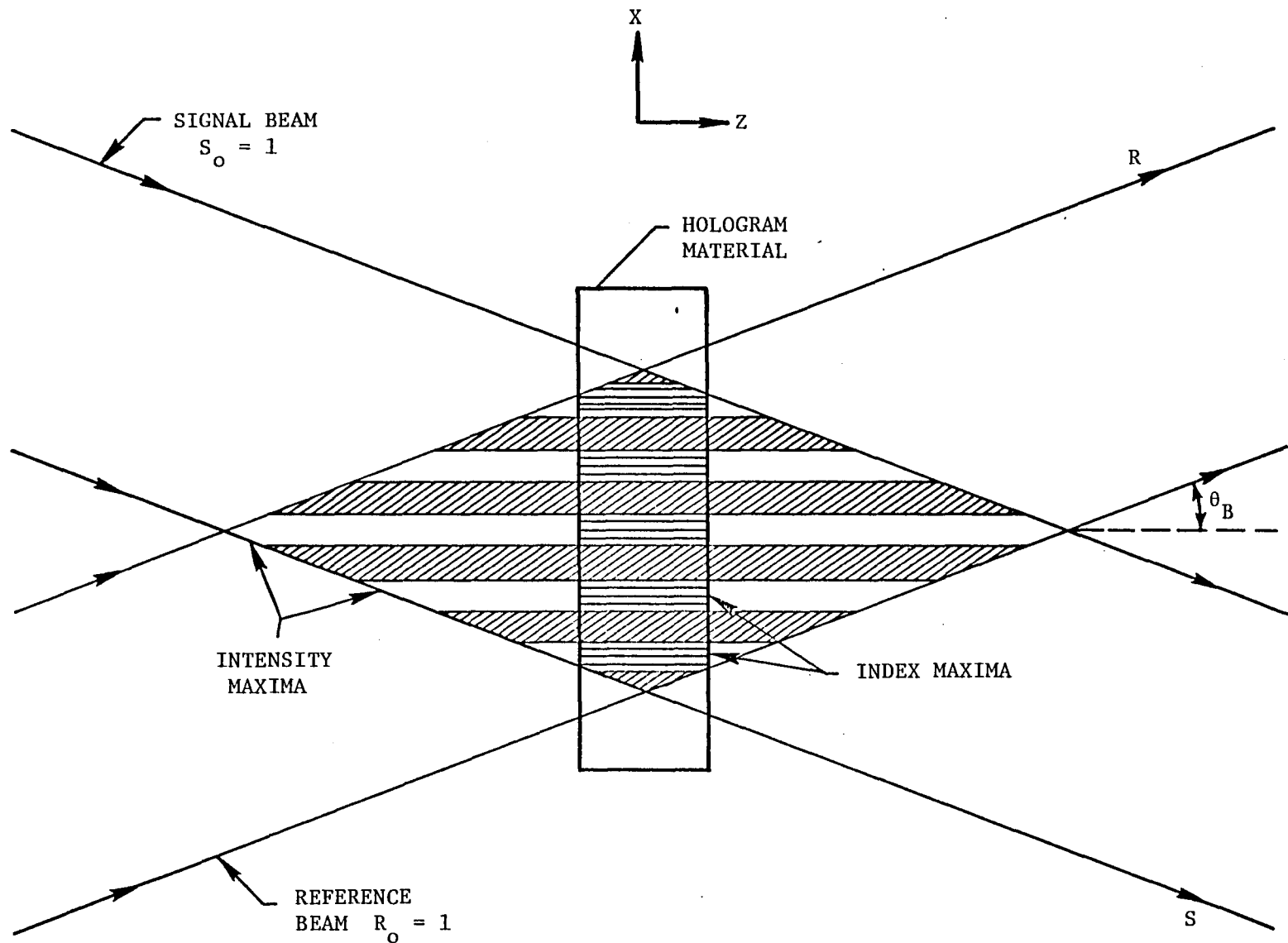


FIGURE II-1. INTERFERENCE PATTERN AND CORRESPONDING REFRACTIVE-INDEX PATTERN AFTER HOLOGRAM FORMATION. INDEX MAXIMA ARE ALIGNED WITH INTENSITY MAXIMA (NO PHASE SHIFT).

requirement that  $S^2 = R^2 = 1$ . (Recall we assumed  $S_0^2 = R_0^2 = 1$  at the hologram input.) This condition is satisfied by Eq. (1) only if  $\psi = \pm \pi/2$ . The correct choice

$$\psi = -\pi/2 \quad (\text{II-2})$$

has been derived by Staebler and Amodei.<sup>(4)</sup>

Let us now apply an external phase shift  $\phi$  to the signal beam in Fig. II-1, so that  $S_0 = 1 e^{i\phi}$  while  $R_0 = 1$  as before. Equation (1) becomes

$$S = (1-\eta)^{1/2} e^{i\phi} - i(\eta)^{1/2} \quad (\text{II-3})$$

$$R = (1-\eta)^{1/2} - ie^{i\phi}(\eta)^{1/2}$$

The output intensities are

$$SS^* = 1 - 2(\eta)^{1/2} (1-\eta)^{1/2} \sin \phi \quad (\text{II-4})$$

$$RR^* = 1 + 2(\eta)^{1/2} (1-\eta)^{1/2} \sin \phi .$$

When  $\phi = \pi/2$ , the signal beam reaches its minimum value and may be described as being holographically "subtracted". In contrast, the reference beam is said to be holographically "added".

Figure II-2 shows the new spatial relationship between the hologram index pattern and the interference pattern. It suggests that in the absence of an external phase shift  $\phi = \pi/2$ , subtraction of the signal beam could have been obtained by displacing the hologram pattern by  $1/4$  fringe, as this accomplishes the same quadrature phase relationship shown in the figure. Materials like  $\text{LiNbO}_3$  for which this phase relationship can be established naturally through the hologram-forming mechanism are those which exhibit self subtraction. In  $\text{LiNbO}_3$ , the dominant hologram-formation mechanism is termed photorefraction, which we now discuss.

#### THE PHOTOREFRACTIVE PROCESS

The term photorefraction designates photoinduced refractive-index changes. In  $\text{LiNbO}_3$  the refractive-index changes arise from the generation of

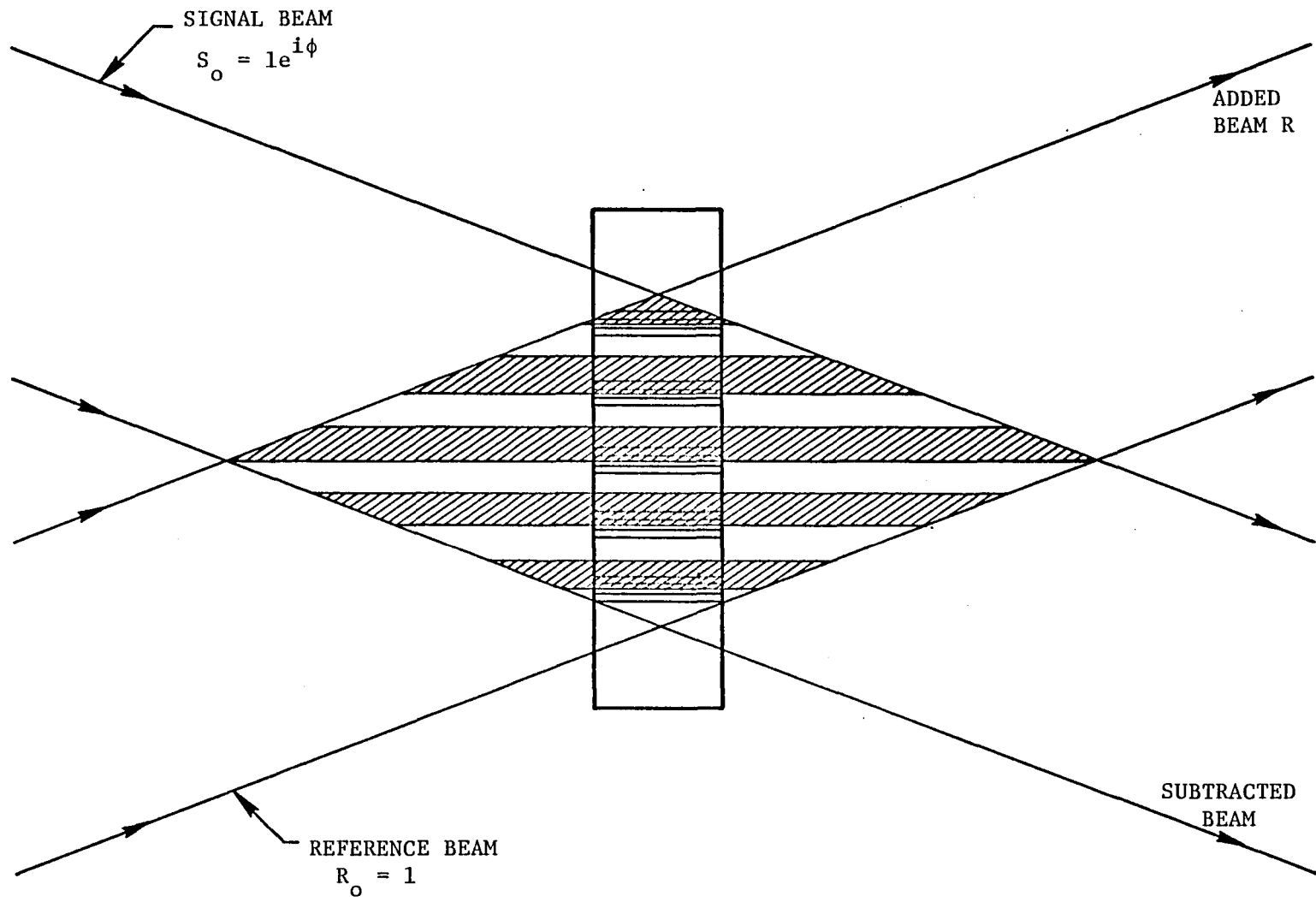


FIGURE II-2. INTERFERENCE PATTERN AND INDEX PATTERN AFTER A  $\pi/2$  PHASE SHIFT APPLIED TO THE SIGNAL BEAM.

a nonuniform distribution of electrons trapped at impurity sites within the crystal.<sup>(5)</sup> When the crystal is illuminated, electrons are excited into the conduction band where they drift and diffuse until they are retrapped.<sup>(6)</sup> For a spatially structured light beam, such as an interference pattern, the general tendency is for the population of trapped electrons to increase in the dark regions of the crystal and to decrease in the illuminated regions. The process is shown schematically in Fig. II-3.

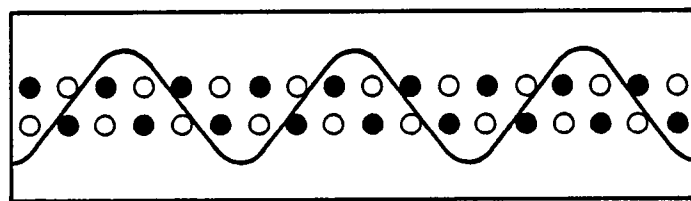
The associated space-charge electric fields produce a refractive-index change by means of the linear electrooptic effect. The process continues uniformly until the space-charge fields become so large that they oppose further migration of electrons.<sup>(7)</sup> Often the fields are as large as  $10^4$  V/cm, corresponding to refractive-index changes greater than  $10^{-4}$ . These index changes are large enough to produce holograms having diffraction efficiencies approaching unity.

#### The Origin of Donors and Traps

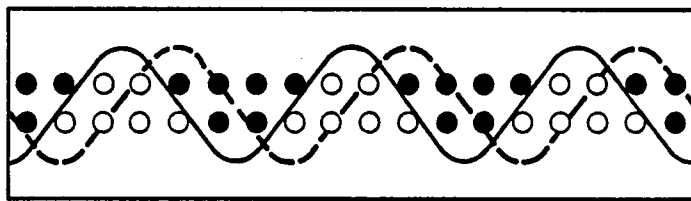
Photorefractive sensitivity is observed to be largest in  $\text{LiNbO}_3$  crystals that have a high concentration of iron.<sup>(5)</sup> Since iron is a naturally occurring impurity in  $\text{LiNbO}_3$ , even samples that are described as nominally pure have sufficient iron for the formation of efficient holograms.  $\text{Fe}^{2+}$  impurities are known electron donors, and  $\text{Fe}^{3+}$  impurities are known traps.<sup>(8)</sup> However, photorefractive effects have also been observed in crystals doped with other ions, such as Cu and Mn,<sup>(9)</sup> and holograms formed by two-photon processes appear to rely on transient photoinduced color centers for sensitization.<sup>(10)</sup> Trapping sites necessary for the formation of long-duration holograms may be associated with crystal imperfections other than impurities, such as oxygen-site vacancies.

#### The Migration of Photoexcited Electrons

After an electron is excited into the conduction band, it may be retrapped at the same location or it may migrate to other regions of the crystal. This migration is partially diffusion controlled, but a more significant mechanism is electron drift associated with a bulk photovoltaic effect.<sup>(5-11)</sup> This effect originates in the pyroelectric nature of the  $\text{LiNbO}_3$



$t = 0$



$t = t_1$

FIGURE II-3. CONCEPTUAL DRAWING SHOWING REDISTRIBUTION OF FILLED TRAPS DURING ILLUMINATION BY AN INTER-FERENCE PATTERN. OPEN CIRCLES ARE UNFILLED TRAPS. CLOSED CIRCLES ARE FILLED TRAPS. SOLID CURVE DESIGNATES INTENSITY VARIATION. DASHED CURVE DESIGNATES REFRACTIVE INDEX VARIATION.

host. Fe impurities are separated from neighboring Nb ions by distances that vary in the positive and negative c-directions. Electrons excited from Fe impurities consequently exhibit a preference to motion in one of the two directions, along which they drift uniformly until they are retrapped. The migration establishes a photovoltage across the illuminated region, the sign of which shows that electron migration occurs along the - c axis. The effect is similar to that which would be observed if the electrons drifted in response to a positively directed electric field. Indeed, the migration can be speeded or slowed by applying a suitable voltage to the crystal. The field required to counteract the photovoltaic effect is found to be about  $5 \times 10^4$  V/cm. (11)

### The Photorefractive Equations

At any point within the crystal, the concentration of conduction electrons  $n$  can be described by a continuity equation. Optical excitation generates conduction electrons, while retrapping, photovoltaic drift, and diffusion remove them. Kim et al<sup>(7)</sup> have employed an equation which appears to account for all relevant processes:

$$\left[ \frac{\partial}{\partial t} + \frac{1}{\tau} - D \frac{\partial^2}{\partial x^2} + \mu \frac{\partial}{\partial x} (E + \bar{E}(x)) \right] n = I(x) N \sigma q / h\nu \quad (\text{II-5})$$

The terms in this equation have the following meaning:

$x$  = the direction parallel to the optic axis;

$\partial n / \partial t$  = rate of change of electron concentration;

$n / \tau$  = rate of electron retrapping;

$D \frac{\partial^2 n}{\partial x^2}$  = spatial derivative of the diffusion current,  $D \partial n / \partial x$ , where  $D$  is the diffusion coefficient;

$\mu \frac{\partial}{\partial x} (En + \bar{E}n)$  = spatial derivative of the drift current, where  $E$  is the effective photovoltaic field,  $\bar{E}$  is the space charge field, and  $\mu$  is the electron mobility;

$I(x) N \sigma q / h\nu$  = rate of generation of conduction electrons per unit volume, where  $N$  is the trapped electron concentration,  $\sigma$  is the absorption cross section,  $q$  is the quantum efficiency for processes resulting in migration,  $h\nu$  = photon energy, and  $I(x)$  = intensity.

For simplicity we eliminate diffusion from further consideration because holographic sensitivity in  $\text{LiNbO}_3$  is much greater for geometries in which both drift and diffusion operate than for geometries in which only diffusion operates. We also neglect the effects of  $\vec{E}$  on electron drift, since it is small during the initial stages of hologram formation in which we have interest. Finally, we neglect  $\partial/\partial t$  in comparison to  $1/\tau$ , since the retrapping time is expected to be on the order of picoseconds while changes in  $n$  from the holographic process occur over a span of seconds. This simplifies Eq. (5) to

$$n + L(\partial n/\partial x) = I(x)N\sigma q\tau/h\nu \equiv g(x)\tau \quad (\text{II-6})$$

where  $L = \mu E\tau$  is the characteristic length that a conduction electron drifts before it is retrapped, and  $g(x)$  is a simplified notation for the generation rate. In the case of illumination by the interference pattern

$$g(x) = g_0(1 + m \cos 2kx\sin\theta) \quad , \quad (\text{II-7})$$

the solution to Eq. (6) is

$$n(x) = n_0 + n_s \sin(2kx\sin\theta) + n_c \cos(2kx\sin\theta), \quad (\text{II-8})$$

$$n_0 = g_0\tau \quad ,$$

$$n_s = g_0\tau m X/(1 + X^2) \quad ,$$

$$n_c = g_0\tau m/(1 + X^2) \quad ,$$

$$X = 2kL\sin\theta \quad ,$$

One particular interest is in the concentration of trapped space charge  $\rho$  described by the continuity equation  $\dot{\rho} = e\mu E\partial n/\partial x$ . After determining  $\rho$  with the help of Eq. (8), Maxwell's equation  $\partial E/\partial x = \rho/\epsilon$  is integrated to obtain the space-charge electric field. The associated refractive index perturbation is  $n_1 = (1/2) n_e^3 r_{33} E$ , where  $n_e = 2.2$  is the extraordinary refractive index of  $\text{LiNbO}_3$ , and  $r_{33} = 30 \times 10^{-12}$  m/V is the appropriate electrooptic coefficient. We find

$$n_1 = n_{10} \cos(2kx\sin\theta - \phi_g) \quad (\text{II-9})$$

$$n_{10} = t(n_e^3 r_{33} / 2) (eLg_o / \epsilon) m \cos\phi_g$$

$$\phi_g = \tan^{-1} 2KL\sin\theta .$$

The phase shift between the hologram index pattern and the optical interference pattern is seen to arise as a natural consequence of electron drift. The value  $\phi_g = \pi/2$  required for self-subtraction can be obtained by a crystal for which  $2kL\sin\theta \gg 1$ ; that is, the drift length is long compared to the hologram fringe spacing.

The value of L can be experimentally increased by reducing the number of empty traps. This can be done by increasing the relative number of filled traps, using reducing treatments of the type described by Phillips and Staebler.<sup>(8)</sup> This was attempted during the program and the results are reported in the next section.

It is worth noting that in crystals for which electron diffusion is the dominant transport mechanism a phase shift  $\phi_g = \pi/2$  automatically occurs. This may be seen by keeping D and eliminating  $\mu$  in Eq. (5), and following procedures similar to those we have already used in analyzing that equation.

#### THEORETICAL ANALYSIS OF SELF-SUBTRACTION

In this subsection we present a theoretical analysis of grating formation in photorefractive  $\text{LiNbO}_3$  for the interesting case of a dominant migration path length L. The treatment is a coupled-wave analysis of Maxwell's equations as they are constrained by the photorefractive equations of the previous subsection. Time-dependent Maxwell's equations are used in view of the slowly varying temporal changes of holograms during their recording. A treatment intermediate to the qualitative picture of self subtraction that introduced the section and the more rigorous derivation presented here is contained in Appendix A.

We assume two coherent beams propagating at angles  $\pm \theta_B$  relative to the Z-axis of the  $\text{LiNbO}_3$  material, as shown in Fig. II-1. These are the

reference and signal beams,  $R$  and  $S$  described by amplitudes  $R$  and  $S$ , phases  $\phi_R$  and  $\phi_S$ , and propagation constant  $\beta$  as follows:

$$R = R(z,t) e^{i\phi_R(z,t)} e^{i\beta\cos\theta z + i\beta\sin\theta x} \quad (\text{II-10})$$

$$S = S(z,t) e^{i\phi_S(z,t)} e^{i\beta\cos\theta z - i\beta\sin\theta x}$$

Note that previously  $R$  and  $S$  were complex and played the role now played by  $\bar{R}$  and  $\bar{S}$ . From this point forward,  $R$  and  $S$  are real quantities. For simplicity the beams are assumed to be polarized in the  $y$  direction. The total electric field  $E = R + S$  satisfies the wave equation

$$\nabla^2 E + k^2 E = 0 \quad (\text{II-11})$$

where  $k = 2\pi n(x,z,t)/\lambda_0$ ,  $n(x,z,t)$  is the refractive index and  $\lambda_0$  is the free-space wavelength. The spatial and temporal variation of the refractive index reflects the fact that the field is writing a hologram by means of the photo-refractive characteristics of the material. Generalizing the result of Eq. (9), we assume a refractive index variation of the form

$$n(x,z,t) = n_0 + n_{10}(z,t) \cos[2kx\sin\theta_B + \phi_R(z,t) - \phi_S(z,t) - \phi_g(z,t)]. \quad (\text{II-12})$$

Here  $n_0$  is the average refractive index. Accordingly, the propagation constant  $\beta$  of Eq. II-10 is given by  $\beta = 2\pi n_0/\lambda_0$ .  $\phi_g(z,t)$  describes the instantaneous phase shift between the hologram index pattern and the optical interference pattern.

By substituting  $k^2 = k_0^2 n^2(z,t)$  into the wave equation along with  $E = R + S$ , we can reduce it to coupled equations for the individual beam amplitudes  $R$  and  $S$ . The procedure for this is exactly that originally employed by Kogelnik.<sup>(12)</sup> Assuming  $n_{10} \ll n_0$  and neglecting all but synchronous terms in the wave equation, we find

$$\partial R/\partial z - i(k_0 n_{10}/2\cos\theta_B) e^{-i(\phi_g + \phi_S - \phi_R)} S = 0 \quad (\text{II-13})$$

$$\partial S/\partial z - i(k_0 n_{10}/2\cos\theta_B) e^{i(\phi_g + \phi_S - \phi_R)} R = 0$$

To complete the formal description of grating formation, it is necessary to develop equations that display the dependence of the grating parameters  $n_{10}$  and  $\phi_g$  on the fields  $R$  and  $S$ . The optical interference pattern at any value of  $z$  and  $t$  is

$$I = n_o (\epsilon_o / 4\mu_o)^{1/2} \{R^2(z,t) + S^2(z,t) + 2R(z,t)S(z,t) \cos[2\beta x \sin\theta_B - \phi_S(z,t) + \phi_R(z,t)]\} \quad (\text{II-14})$$

This interference pattern excites trapped electrons into the  $\text{LiNbO}_3$  conduction band where they migrate antiparallel to the crystal's optical axis as described above. Consider electrons initially in a volume element  $\Delta V = \ell_y \Delta x \Delta z$ , where  $\ell_y$  is the length of the hologram in the  $y$  direction. The number of electrons excited in an interval  $\Delta t$  is called  $\Delta N_-$ , where

$$\Delta N_-(x,z,t) = (N_o \ell_y \Delta x \Delta z) F_o \sigma \Delta t \eta [1 + m \cos(2\beta x \sin\theta_B - \phi_S + \phi_R)]. \quad (\text{II-15})$$

In this equation  $N_o$  is the density of trapped electrons,

$$F_o = [n_o (\epsilon_o / 4\mu_o)^{1/2} (R^2 + S^2)] / h\nu \quad (\text{II-16})$$

is the average flux density of the beam,  $h\nu$  being the energy per photon,  $\sigma$  is the absorption cross section,  $\eta$  is the quantum efficiency for the generation of conduction electrons, and

$$m = n_o (\epsilon_o / 4\mu_o)^{1/2} 2RS / F_o h\nu \quad (\text{II-17})$$

is the visibility of the interference pattern. The result of photorefractive migration is to distribute these electrons into new volume elements  $\ell_y \Delta x \Delta z$  centered at  $x' > x$ . The fact that these electrons are lost to the original volume element is indicated by use of the notation  $\Delta N_-$ . However, these electrons are replaced by electrons generated at  $x' < x$  which drift into the volume element at  $x$ . This contribution is

$$\Delta N_+(x,z,t) = \int_{-\infty}^x \frac{dx'}{L} e^{-(x-x')/L} \Delta N_-(x',z,t) \quad (\text{II-18})$$

where  $L$  is the migration path length, and the exponential term accounts for the decreasing contribution from increasingly distant volume elements.

The total change in the number of trapped electrons at  $x$  is  $\Delta N = \Delta N_+ - \Delta N_-$ . An expression for  $\Delta N$  is obtained by carrying out the integral of Eq. (18) and by subtracting from the result the expression of Eq.(15). We find

$$\Delta N = N_o (\ell_y \Delta x \Delta z) F_o \sigma \eta \Delta t m (1 + K^2 L^2)^{-1} KL \quad (\text{II-19})$$

$$\{-KL \cos(Kx + \phi) + \sin(Kx + \phi)\} ,$$

where we have introduced the grating vector magnitude  $K \equiv 2\beta \sin \theta_B$  and the phase difference  $\phi \equiv \phi_R - \phi_S$ .

The redistribution of electrons described by Eq. (19) produces an incremental space-charge electric field  $\Delta E$  consistent with the Maxwell equation

$$\partial(\Delta E)/\partial x = \Delta \rho / \epsilon_o \kappa , \quad (\text{II-20})$$

$$\Delta \rho = -e \Delta N / (\ell_y \Delta x \Delta z) ,$$

where  $\Delta \rho$  is the space charge density and  $\kappa$  is the dielectric constant. The space-charge field  $\Delta E$  in turn causes a proportional refractive index change of electrooptic origin,  $\Delta n$ , given by

$$\Delta n = \frac{1}{2} n_o^3 r \Delta E , \quad (\text{II-21})$$

where  $r$  is the appropriate electrooptic coefficient. By inserting Eq. (19) into Eq. (20), integrating, and then substituting the result for  $\Delta E$  into Eq. (21) we find

$$\Delta n(x, z, t) = \Delta t (n_o^3 r / 2) (eL / \epsilon_o \kappa) N_o F_o m \sigma \eta (1 + K^2 L^2)^{-1/2} \quad (\text{II-22})$$

$$\cos(Kx + \phi - Q) ,$$

where  $Q = \tan^{-1} KL$  is the photorefractive phase shift obtained previously. The term  $F_{0m}$  on the right-hand side of this equation is related to the field amplitudes  $R$  and  $S$  by Eq. (17), which we restate:

$$F_{0m} = n_0 (\epsilon_0 / \mu)^{1/2} (h\nu)^{-1} R(z,t)S(z,t) \quad (\text{II-23})$$

A differential equation relating the refractive index of the material to the fields is obtained by inserting this result into Eq. (22), dividing by  $\Delta t$ , and letting  $\Delta t$  become infinitesimal. We find

$$\partial n(x,z,t) / \partial t = A R(z,t)S(z,t) \cos(Kx + \phi_R - \phi_S - Q) \quad (\text{II-24})$$

$$A = (n_0^4 r / 2) (eL / \kappa) (\lambda_0 / h) N_0 \sigma n (1 + K^2 L^2)^{-1/2} .$$

It is convenient to rewrite this result in the form

$$\partial n / \partial t = ARS \cos(Q - \phi) \cos Kx + ARS \sin(Q - \phi) \sin Kx . \quad (\text{II-25})$$

For comparison, Eq. (12) defining  $n(x,z,t)$  is rewritten

$$n = n_0 + n_{10} \cos(\phi_g - \phi) \cos Kx + n_{10} \sin(\phi_g - \phi) \sin Kx . \quad (\text{II-26})$$

By taking the time derivative of this expression and comparing the coefficients of the  $\cos Kx$  and  $\sin Kx$  terms that result with those of Eq. (25), we can make the identification

$$\partial / \partial t (n_{10} e^{i(\phi_g - \phi)}) = ARS e^{i(Q - \phi)} . \quad (\text{II-27})$$

This equation together with Eq. (13) provides the information we require to obtain the field and refractive-index variations encountered during photorefractive grating formation. Analysis of the three complex equations is facilitated by rewriting them as six real equations for the quantities  $R, S, \phi_R, \phi_S, n_{10}$  and  $\phi_g$ . This is straightforward to carry out. The resulting equations are

$$R_z - BSn_{10}\sin\phi_g = 0 \quad (a) \quad (II-28)$$

$$S_z + BRn_{10}\sin\phi_g = 0 \quad (b)$$

$$R(\phi_R)_z - BSn_{10}\cos\phi_g = 0 \quad (c)$$

$$S(\phi_S)_z - BRn_{10}\cos\phi_g = 0 \quad (d)$$

$$(n_{10})_t - ARScos(Q-\phi_g) = 0 \quad (e)$$

$$n_{10}(\phi_g-\phi)_t - ARSsin(Q-\phi_g) = 0 \quad (f)$$

We have introduced  $B \equiv k_o/2\cos\theta_B$ , and we have employed subscripts  $z$  and  $t$  to designate  $\partial/\partial z$  and  $\partial/\partial t$ , respectively. The initial conditions and boundary conditions to use in solving these equations are as follows:

$$R(0,t) = R(z,0) = R_o \quad (II-29)$$

$$S(0,t) = S(z,0) = S_o$$

$$\phi_R(0,t) = \phi_R(z,0) = 0$$

$$\phi_S(0,t) = \phi_S(z,0) = 0$$

$$\phi_g(0,t) = \phi_g(z,0) = Q$$

$$n_{10}(z,0) = 0$$

In general, these equations must be solved numerically. There are, however, two special cases for which analytic solutions are available. These are the cases  $Q = 0$  and  $\pi/2$ . In the former, we also require  $R_o = S_o$ . In the latter, we require  $R_o \gg S_o$ . We now consider these special cases, and, in closing, the general case.

Case I.  $Q = 0, R_o = S_o$ . With  $Q = \phi_g(z,0) = 0$ , Eqs. (28a) and (28b) show that there is no tendency for  $R$  and  $S$  to deviate from their initial values

$R_0$  and  $S_0$ , at least for short writing times. The result is that  $\phi_R$  and  $\phi_S$  increase in a parallel manner [Eqs. (28c) and (23d)] with the difference  $\phi = 0$  maintained. This forces  $\phi_g$  to remain at zero in accord with Eq. (28f). The same argument can be employed to describe successive small increments of writing time. The net result is

$$\begin{aligned} R(z,t) &= R_0 & \text{(II-30)} \\ S(z,t) &= S_0 \\ \phi_R(z,t) - \phi_S(z,t) &= 0 \\ n_{10}(z,t) &= AR_0 S_0 t \\ \phi_g(z,t) &= 0 \end{aligned}$$

As time increases, the space-charge fields eventually assume a major role in governing the redistribution of photoexcited carriers. This has not been taken into account, and is the source of the unphysical result that  $n_{10}$  is proportional to  $t$  at all writing times. However, high diffraction efficiency gratings can be recorded in times for which Eq. (30) is valid.

Case II  $Q = \pi/2, R_0 \gg S_0$ . With  $Q = \phi_g(z, 0) = \pi/2$ , Eqs. (28c) and (28d) indicate no initial change in  $\phi_R$  or  $\phi_S$ . This is true even though there is a change in  $R$  and  $S$ , with  $R$  increasing from  $R_0$ , and  $S$  decreasing from  $S_0$ . By Eq. (28f), the stability of  $\phi_R - \phi_S$  insures the continuation of the initial condition  $\phi_g = \pi/2$ , so that the same argument continues to apply for all writing times. The coupled Eqs. (28) simplify to

$$\begin{aligned} R_z - BSn_{10} &= 0 & \text{(a')} & \text{(II-31)} \\ S_z + BRn_{10} &= 0 & \text{(b')} \\ (n_{10})_t - ARS &= 0 & \text{(e')} \end{aligned}$$

To obtain a single partial differential equation for  $S$ , we make use of the energy-conservation condition

$$R^2 + S^2 = R_0^2 + S_0^2 \equiv U_0^2 \quad , \quad (\text{II-32})$$

which may be derived from Eqs. (31a') and (30b'). By substituting  $R = (U_0^2 - S^2)^{1/2}$  in Eq. (31b'), dividing by  $(U_0^2 - S^2)^{1/2}$  to segregate terms containing S from terms containing  $n_{10}$ , differentiating with respect to time, and rearranging terms, we obtain

$$(U_0^2 - S^2)S_{zt} + SS_z S_t + AB S(U_0^2 - S^2)^2 = 0 . \quad (\text{II-33})$$

This may be converted to an ordinary differential equation by introducing the variable  $w = ABzt$ . The result is

$$(wS_{ww} + S_w)(U_0^2 - S^2) + wSS_w^2 + S(U_0^2 - S^2)^2 = 0 . \quad (\text{II-34})$$

This equation is valid for all initial values of  $U_0$  and  $S_0$ . However an analytic solution is obtained when  $U_0^2 \gg S^2$ , that is, when most of the energy is confined to the reference beam. On the basis of this assumption we neglect terms that are quadratic in S or higher in Eq. (34), with the resulting simplification:

$$wS_{ww} + S_w + S = 0 . \quad (\text{II-35})$$

This is a member of the class of equations solved by Bessel functions.<sup>(13)</sup> The solution is

$$S(z,t) = S_0 J_0 [2(ABzt)^{1/2}] . \quad (\text{II-36})$$

An example of the shape of the curve  $(S/S_0)^2$  is indicated in Figs. II-4 and II-5 along with numerically generated curves obtained from the computer solution of the general equations, Eq. (28), which we now discuss.

Case III. The General Case. A FORTRAN computer program was developed to solve Eq. (28). The numerical method employed was that of finite differences, modified to insure conservation of energy of reference and signal beams. The program has not been optimized. Rather precision of results has been achieved by the procedure of using sufficiently small increments of space and

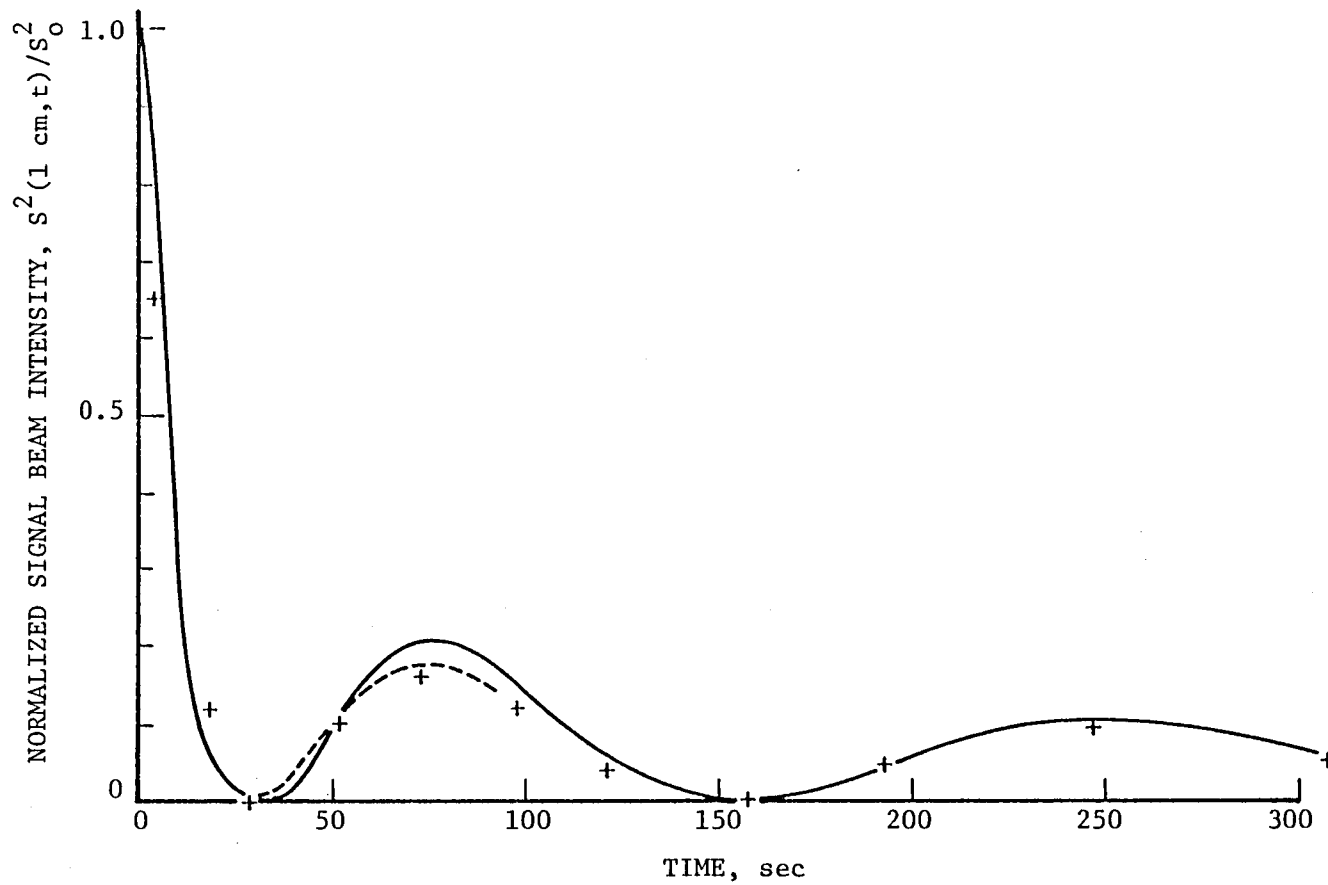


FIGURE II-4. SIGNAL-BEAM INTENSITY VS RECORDING TIME. SOLID CURVE: COMPUTED FOR  $(S_0 - R_0)^2 = 0.01$ ,  $Q = 1.5$ . CROSSES: APPROXIMATE BESSEL-FUNCTION SOLUTION. DASHED CURVE: COMPUTED WITH GREATER PRECISION.

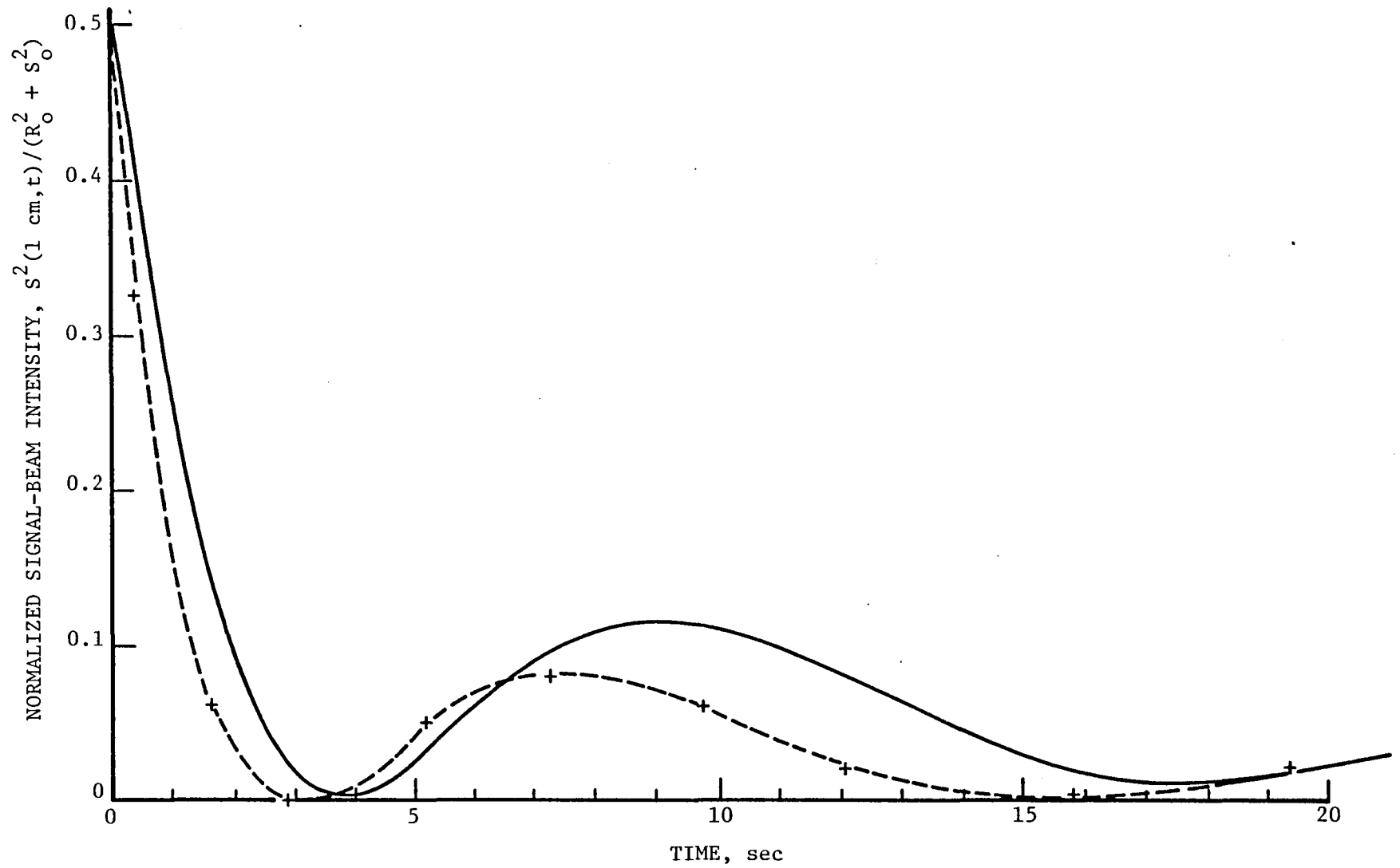


FIGURE II-5. SIGNAL-BEAM INTENSITY VS RECORDING TIME. SOLID CURVE: COMPUTED FOR  $s_0^2 = R_0^2 = 1/2$ ,  $Q = 1.4$ . DASHED CURVE: BESSEL FUNCTION APPROXIMATION.

time to integrate the coupled equations. The difficulty in implementing a program to solve the given system may be inferred from an examination of Eq. (28d). As the S-beam amplitude decreases toward zero during subtraction, the spatial rate of change of the phase  $\phi_S$  becomes very large. This jeopardizes the precision of the calculation unless care is taken. Problems that we encountered in this regard prevented us from performing a very detailed study of the implications of Eq. (28). We have, however, identified two important features: (1) Slight reduction of the parameter  $Q$  from  $\pi/2$  does not seriously degrade the crystal's capability for performing self subtraction; and (2), self subtraction is largely independent of the initial beam ratio  $(S_o/R_o)$ .

Figure II-4 shows the computer generated self-subtraction curve for the case  $(S_o/R_o)^2 = 10^{-2}$  and  $Q = 1.5$ . The value for  $A$  was  $10^{-6} \text{ sec}^{-1}$ ; and for  $B$ ,  $4.971 \mu\text{m}^{-1}$ . Crosses placed close to the computed curve show the corresponding value of the Bessel-function approximation given by Eq. (36). There is some evidence that the agreement between the two calculations is even better than shown. Over a limited range that was tested, the computed curve approaches the Bessel-function curve as more precision is obtained from the calculation (dashed curve in Fig. II-4).

In Fig. II-5, we present the computer-generated results for the case  $(S_o/R_o)^2 = 1$  and  $Q = 1.4$ . We find, first of all, a secondary maximum that is about 20% of the initial intensity. This was also the case for the beam ratio  $(S_o/R_o)^2 = 10^{-2}$ . The nature of the subtraction curve does not, therefore appear to depend strongly on beam ratio. One noticeable difference between the computed curves of Figs. II-4 and 5, however, is the extent to which minima approach the baseline. The approach is closer in the case of the smaller beam ratio of Fig. II-4, which incidentally pertains to a value of  $Q$  that is closer to the ideal subtraction value  $\pi/2$ . For the curve of Fig. II-5, the second minimum is significantly further from the baseline than the first minimum. This could be an indication that the long-term signal intensity does not approach zero as the Bessel-function approximation suggests. We looked for this instability experimentally but did not find it. Details of the experiment will be provided in Sec. IV. It is possible that photorefractive saturation effects not accounted for in the present theory could prevent instabilities in the subtraction process from becoming evident, thus explaining our experimental result.

Figure II-5 shows, in addition to the computed curve, the Bessel-function subtraction curve obtained from the theory for the case of a small beam ratio and  $Q = \pi/2$ . At small times, differences in the computed and Bessel curves reflect differences in the beam ratio. As subtraction progresses, the beam ratio becomes small even though it was not small initially. We therefore expect and observe oscillatory behavior similar to that shown by the Bessel-function curve of Fig. II-5. Failure of the computed curve to reach the baseline is probably more an indication of the choice  $Q = 1.4$ , that is,  $Q$  less than  $\pi/2$ , than it is an indication of beam ratio. If this is true and if the failure of the computed curve to reach the baseline is an indication of self-subtraction instability, then the time required for instability to become evident probably decreases as the deviation of  $Q$  from the ideal subtraction condition,  $Q = \pi/2$ , increases. This is a question to be addressed in future theoretical work on self subtraction, along with changes in the theoretical model to account for photorefractive saturation effects that could limit the appearance of instabilities and smooth the oscillations of the subtraction curves.

Thus far our treatment of the general Eq. (28) has addressed only the evolution of beam intensity during the subtraction process. In concluding this section we discuss the beam phase  $\phi = \phi_R - \phi_S \cong -\phi_S$ . In the limiting case described by the solution

$$S(z,t)/S_0 = J_0[2(ABzt)^{1/2}] \quad , \quad \text{II-37}$$

zero crossings of the Bessel function correspond to points where the phase of the signal beam,  $\phi_S$ , jumps by  $\pi$ . In the general case the change in phase is continuous, but rapid variations occur at times when the signal beam intensity is at a minimum. Figure II-6 and II-7 show the computed variations of the phase  $\phi_S(1 \text{ cm}, t)$  for the initial conditions used to generate Figs. II-4 and II-5, respectively. Arrows designate those times at which  $S^2$  is a minimum. In the case of Fig. II-6, for  $S_0/R_0 = 1/10$  and  $Q = 1.5$ , the off-scale values of  $\phi_S$  near the first minimum of  $S^2$  result from imprecise computation in that region. A dashed curve shows more precise values.

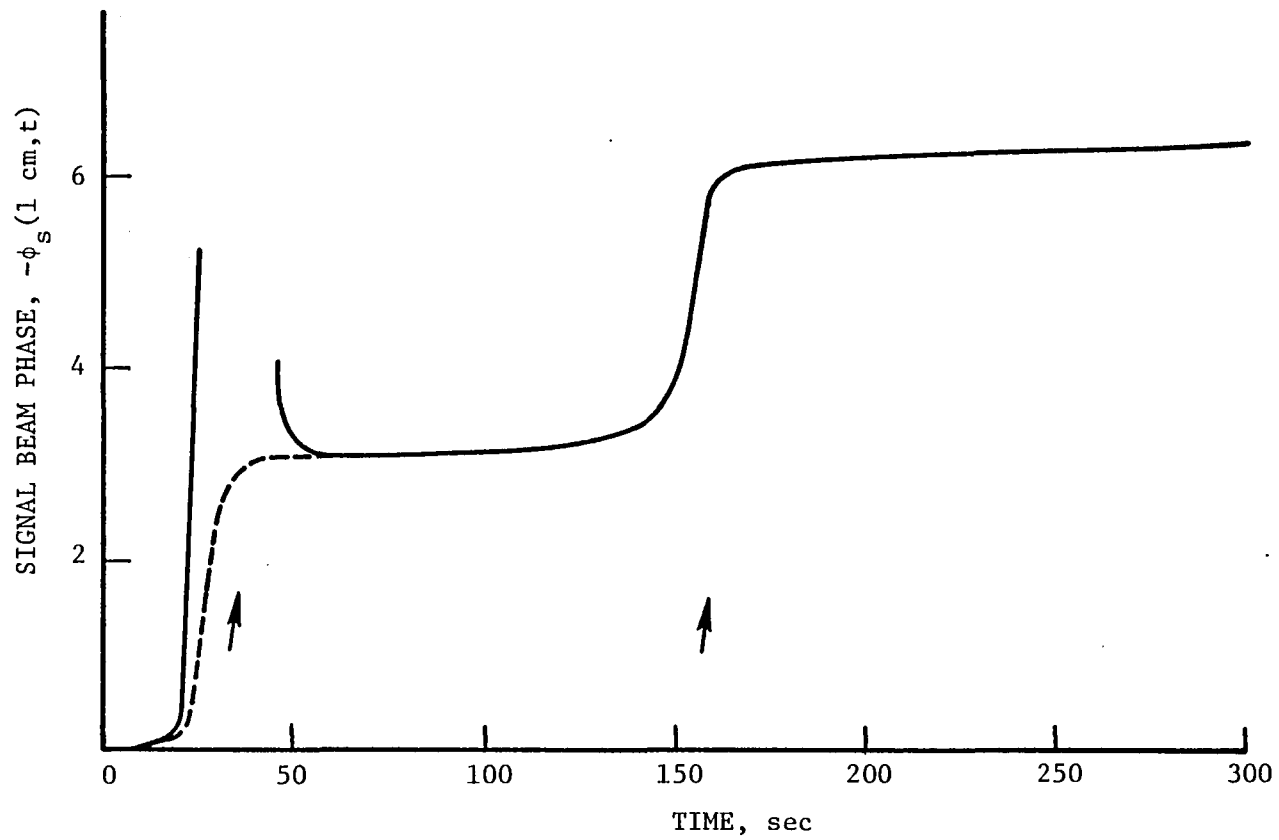


FIGURE II-6. SIGNAL-BEAM PHASE VS RECORDING TIME FOR  $(S_0/R_0)^2 = 0.01$  AND  $Q = 1.5$ . ARROWS DESIGNATE MINIMA OF SIGNAL-BEAM INTENSITY. DASHED PORTION OF CURVE SHOWS RESULTS OF MORE PRECISE COMPUTATION.

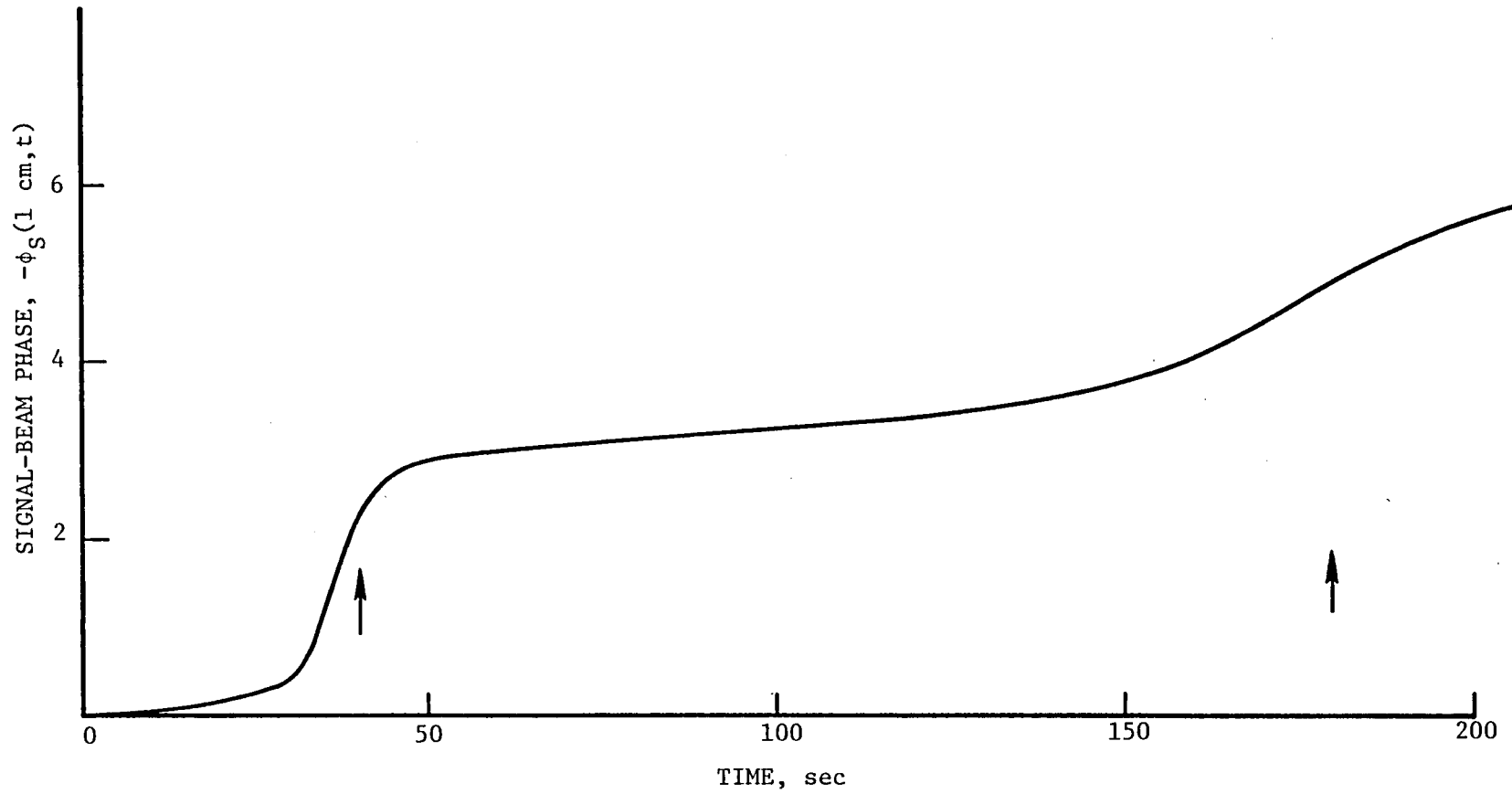


FIGURE II-7. SIGNAL-BEAM PHASE VS RECORDING TIME FOR  $S_0^2 = R_0^2 = 1/2$ ,  $Q = 1.4$ .  
ARROWS DESIGNATE MINIMA OF SIGNAL-BEAM INTENSITY.

STATUS OF THE THEORETICAL UNDERSTANDING OF  
HOLOGRAM FORMATION IN  $\text{LiNbO}_3$

The level of the theory presented in this section is the simplest that one can appeal to and still describe beam-interaction effects such as those associated with self subtraction. This is evidenced by the fact that the very complicated photorefractive effect is reduced in this work to a single parameter  $L$ , the electron drift path length. This was appropriate because any attempt to fit experimental results to a theoretical model should begin with the simplest model possible. The reader should understand, however, that considerable literature on the dynamics of hologram formation in photorefractive materials exists, and that much of it employs more sophisticated modeling than that described here. We cite as representative work by Gaylord and colleagues at Georgia Tech<sup>(14,15)</sup> and work by Young and colleagues at the University of British Columbia<sup>(6,15,16)</sup>. This is in addition to the research cited earlier done by Tittel and colleagues at Rice University.<sup>(7)</sup> Other authors have also noted the exchange of energy between writing beams during hologram formation in photorefractive materials.<sup>(4,17-19)</sup> One group has noted the potential of holographic self addition and self-subtraction for use in optical image processing applications.<sup>(17)</sup>

### III. EXPERIMENTAL METHODS FOR THE STUDY OF SELF-SUBTRACTION

This section concerns the experimental methods used in the program. Actual results are described in detail in Sec. IV. We now limit discussion to the types of samples studied, the geometry of the experiments, the procedures and problems encountered in taking data, and sample preparation techniques.

#### THE USE OF OPTICAL WAVEGUIDE SAMPLES

Perhaps the most significant procedural difference between this program and other programs that have dealt with photorefractive properties of  $\text{LiNbO}_3$  is the use of optical waveguide samples rather than bulk samples.<sup>(4,8-11)</sup> One of several good reasons for using waveguides is that potential applications of self-subtraction are attractive to consider implementing in an integrated optical format.<sup>(3)</sup> Using this format, one has the advantages of achieving a high beam intensity using low-optical powers and also the advantages of writing holograms that are up to 15-mm thick in sturdy yet thin slabs that need be polished on only one side. These features allow for the formation of efficient holograms using 0.633- $\mu\text{m}$  recording wavelength, which is non-optimum, in writing times of about two minutes. Additionally, heat treatments to modify the photorefractive characteristics of the waveguide do not require the tens and even hundreds of hours of thermal equilibration time that thick samples for conventional volume holography do.<sup>(8)</sup> All these features result from the fact that in the integrated optical format only the top few microns of material are exposed to the waveguided beam. An assumption that we make is that the nature of photorefractivity is fundamentally the same within the top few microns of material as it is everywhere within the sample volume. Although this is an assumption that should be checked, we have been comfortable with it in view of the fact that we observe similar characteristics for holograms in both integrated optical and conventional 3-D optical formats.

### THE SAMPLE GEOMETRY

Figure III-1 shows the sample-optical beam configuration typical of that employed in our experiments. Two coherent beams of 0.633- $\mu\text{m}$  wavelength radiation from a He-Ne laser are coupled into the  $\text{LiNbO}_3$  waveguide using a 10-mm wide coupling prism. Interference fringes are established in the overlap region which run parallel to the line bisecting the guided beams and perpendicular to the optical axis. The light is TE polarized; that is, the electric vector is in the plane of the waveguide. Usually the light is in the  $\text{TE}_0$  waveguide mode. It is important that both beams occupy the same mode to establish a high-contrast interference pattern and thereby to increase the rate of hologram formation.

The signal beam is the narrower of the two beams shown in Fig. III-1. It is typically formed by aperturing to 1-mm width a beam that is an attenuated mirror image of the broad reference beam used in the experiment. This geometry maximizes the path length and the spatial uniformity of the hologram. Moreover, it minimizes the effects associated with the diamond-shaped hologram region that results from the use of finite beams. Diamond-shaped holograms exhibit recording characteristics that have special features associated with their geometry. (20,21) This would complicate the interpretation of our results so we minimize the effects by using the wide-beam narrow-beam geometry of Fig. III-1.

In order to use the theory of self-subtraction to analyze our experimental data and thereby obtain values for photorefractive parameters, it is necessary to know the intensity of light in each waveguided beam. This is a situation in which the integrated optical format presents a problem not encountered with the conventional bulk optical format. Generally the power throughput of a prism-input and-output coupled waveguide is in the range 1% - 10%. The power in the waveguide is indicated by the input coupling efficiency alone. This could be as small as the throughput itself or as large, approximately, as the square root of the throughput. Even if the power in the waveguide were known accurately, the intensity varies spatially with depth from the waveguide surface according to the mode profile, and an

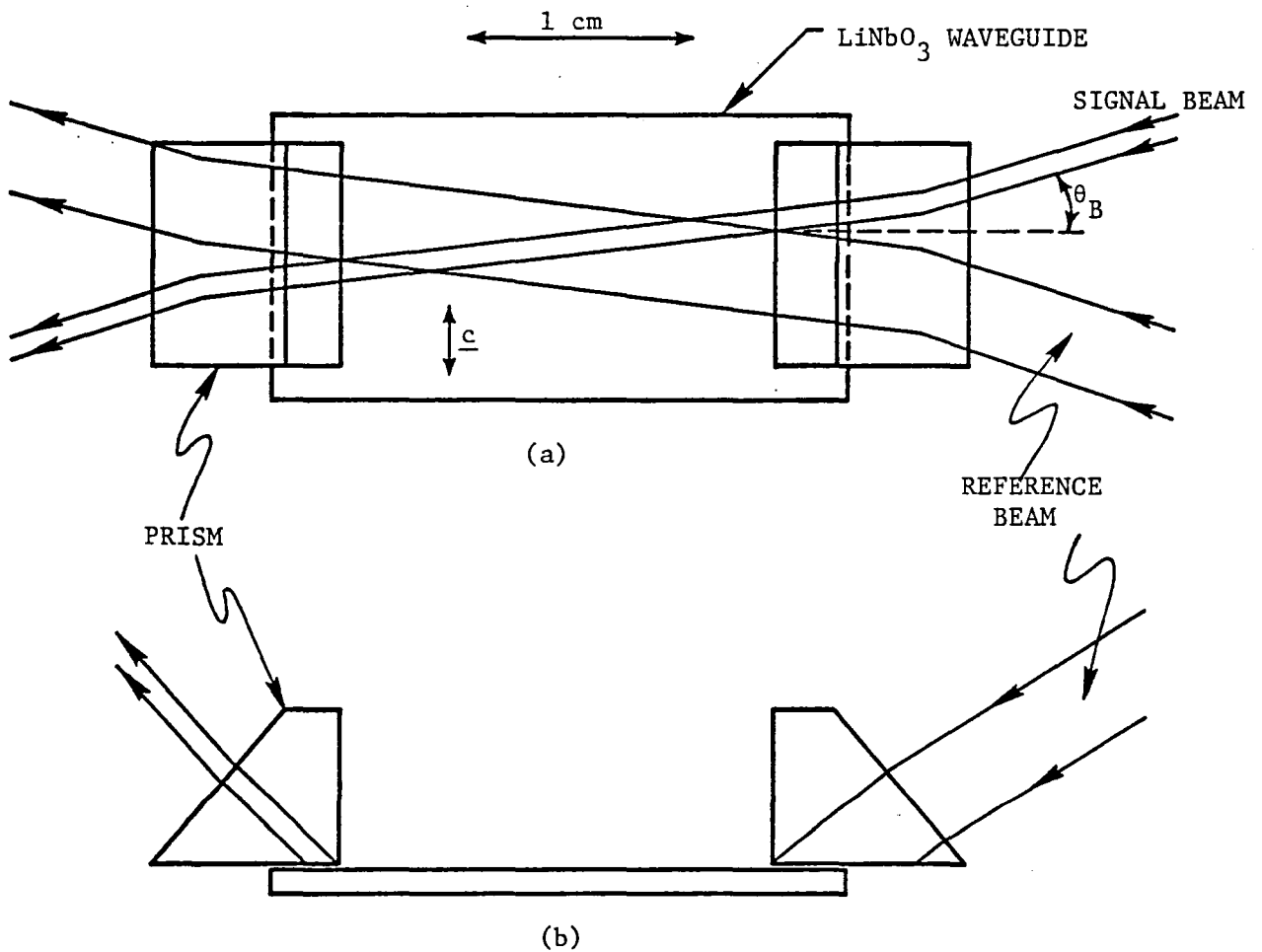


FIGURE III-1. THE SAMPLE-OPTICAL BEAM CONFIGURATION.  
 (a) TOP VIEW. (b) SIDE VIEW.

appropriate average intensity would have to be computed to use in the formulas of the previous section. The net effect is a rather large uncertainty when our experimental results are applied to the estimation of parameters in the theory. For this reason we have not made parameter determination an important part of our experiments. Rather, our interest has been in the shape of the curves describing signal-beam output intensity as a function of time, and in a comparison of experimental and theoretical curve shapes. The curves scale with optical intensity but, in the absence of nonlinear effects, do not change in shape with changes in optical intensity.<sup>(2)</sup> This was verified to our satisfaction by an experiment conducted during the program.

For those who may wish to reproduce our experiments, we note that typical values of input power in the approximately 4-mm diameter reference beam were 5 mW measured before the input coupling prism and 20  $\mu$ W measured after the output coupling prism. Taking the latter number as a lower estimate of power in the waveguide and employing an approximate beam cross section of 4 mm x 5  $\mu$ m, the average intensity of the waveguided beam is found to be 0.1W/cm<sup>2</sup>. This is several orders of magnitude below the intensities observed to cause significant nonlinear photorefractive effects.<sup>(22)</sup>

One final aspect of the sample geometry shown in Fig. III-1 has to do with the period of the hologram fringes, called  $\Lambda$ , and its relation to the Bragg angle,  $\theta_B$ . The relevant formula is

$$\Lambda = \lambda_o / 2 \sin\theta_B \quad \text{III-1}$$

where  $\lambda_o$  is the free-space wavelength of the writing light, and  $\theta_B$  is measured external to the sample. The same formula would apply if  $\theta_B$  were measured in the waveguide sample, except that  $\lambda_o$  would then be replaced by  $\lambda$ , the wavelength in the material. The changes in  $\theta_B$  and  $\lambda_o$  caused by refraction exactly cancel each other with the result that an identical value for  $\Lambda$  is calculated. In order to be specific, we take  $\theta_B$  to be the Bragg angle measured external to the waveguide, prior to input coupling. For a typical value  $\theta_B = 15^\circ$ , the hologram period is  $\Lambda = 1.22 \mu\text{m}$ .

## THE ARRANGEMENT OF EXPERIMENTAL APPARATUS

Figure III-2 shows the overall arrangement of the self-subtraction experiment. A variable beam splitter was used to divide a collimated laser beam of approximately 4 mm diameter into signal and reference beams. The beam intensity ratio was in the range from 100:1 to 1:1, with the signal beam identified as the weaker of the two. Four mirrors were used to recombine the beams at the  $\text{LiNbO}_3$  sample as shown in the figure. The additional two mirrors over the minimum two required facilitated the adjustments needed to couple both beams into the waveguide at once. One mirror was mounted on a piezoelectrically translated stage to accomplish a voltage controlled phase shift. This could then be used to test the sensitivity of a self-subtraction hologram to small phase shifts such as those that might someday contain signal information in a practical device. Alternatively, a phase shift equal to  $\pi$  could be applied to peak the intensity of the subtracted beam. The ratio of the peaked signal to the previous subtracted signal is called the contrast ratio and is a figure of merit of the subtraction process. Moreover, the sudden application of a phase shift is used as the initial step in evaluating the ability of the sample to recycle; that is, the ability to record new self-subtraction holograms on top of old ones without the need for optical or thermal erasure.

A vertical 1-mm wide slit was placed in the signal beam before coupling into the waveguide to reduce the width of the beam without changing its intensity. Beam ratios were measured by use of a power meter placed in the signal beam prior to aperturing. Consequently, these ratios refer to relative intensity in the waveguide and not relative power. The slit was found to block approximately 70% of the incident power from the signal beam.

## DATA ACQUISITION

The typical approach to data acquisition that we employed is described as follows: The output signal beam was directed to a UDT power meter for detection. The analogue output from the power meter was used to drive

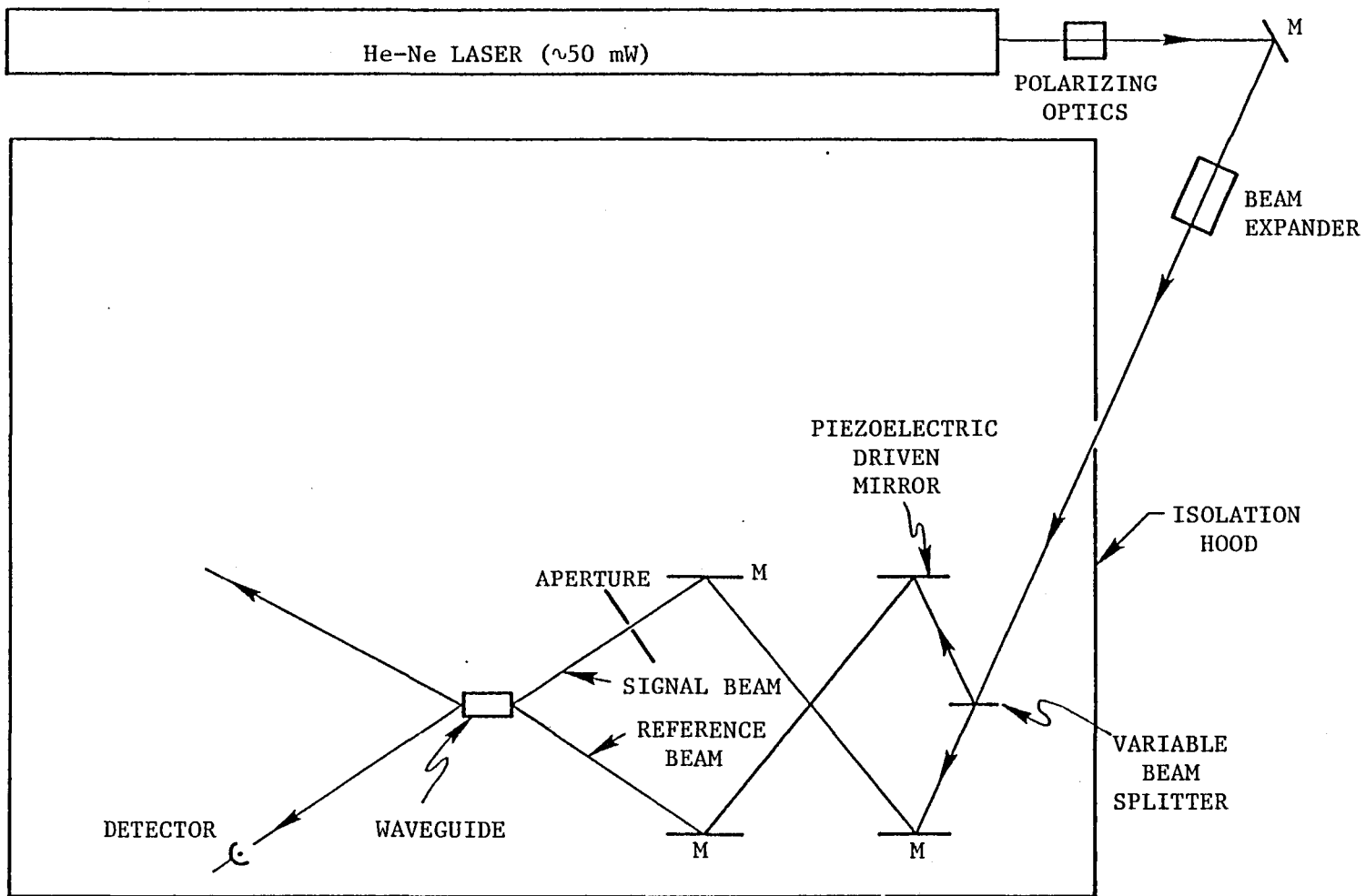


FIGURE III-2. EXPERIMENTAL ARRANGEMENT FOR SELF-SUBTRACTION STUDIES

the y-axis of an x-y recorder while the x-axis position was changed at a constant rate commensurate with the hologram-formation time constant. This produces the desired permanent record of the evolution of the hologram. The method is attractive in its simplicity, yet there are several sources of optical errors that have to be taken into account.

First of all, scattering in the waveguide causes a noticeable fraction of the output reference and signal beams to fan out. The strength of the scattered component is further enhanced by photorefraction. The net effect is that a portion of the signal beam misses the finite collection aperture of the power meter and is not detected. An associated problem is that a scattered portion of the reference beam can reach the detector and be recorded as signal. We have ignored the first problem, as is acceptable provided that the fraction of scattered signal power is a constant in time. The second problem is more severe because it prevents us from measuring unscattered signal power below a certain background level. Since the minimum signal power obtained during self-subtraction is a measure of the quality of the effect, the background scattering should be eliminated as much as possible, and any residual scattering should be measured to be sure that it is not a factor in the experiment.

Generally, background scattering is reduced by moving the detector further from the waveguide. Residual levels of background scattering are conveniently measured by either of several methods. In one, the signal beam is blocked and the scattering from the reference beam is measured as background. This method fails if a hologram exists in the sample when the measurement is made. In this case light diffracted by the hologram is incident on the detector. Since this is not scattered background light, an erroneous reading is obtained. In addition the technique suffers from the fact that background scattering from the signal beam is not recorded, although this component would be negligible in most experiments where the beam ratio is on the order of 10:1 or 100:1.

A second method for measuring background scattering is valid when both reference and signal beams illuminate the sample and even when a hologram has been recorded. In this method, the detector is simply raised and lowered relative to its initial position in the path of the signal beam.

The average reading in the raised and lowered positions is an indication of the background level at the intermediate position occupied by the signal beam. One of the two types of background-level measurements we have discussed should be made in all experiments in which the minimum power in the subtracted beam is a quantity of interest.

In addition to the problem of background scattering, another source of experimental error to be considered is air turbulence. This effect causes fluctuations in the optical lengths of the reference and signal beam paths. A legitimate self-subtraction hologram cannot be recorded unless the corresponding phase fluctuations are much less than  $\pi$ . To achieve this, the experiment of Fig. III-2 was housed beneath a rectangular frame enclosure covered with transparent polyethylene sheet.

#### A PHASE-TRACKING EXPERIMENT

Figure III-3 shows a modification of the basic experimental set up that was devised to track phase changes of the signal beam as a self-subtraction hologram was recorded. This was done as a test of the theory of Sec. II. Figures II-6 and 7 of that section indicate that as the subtracted beam intensity approaches zero, the temporal rate of change of the phase of that beam becomes large. Measurements of the self-subtraction intensity alone contain no phase information, so the modification shown in Fig. III-3 was established to gather this information. We desired to measure any rapidly occurring phase changes that might occur as the self-subtracted intensity became small.

Figure III-3 shows that part of the reference beam is redirected by a beam splitter and mixed with a portion of the output signal beam. A photomultiplier is set up to detect light from the resulting fringe pattern. An aperture is used to limit the field of view to a width small compared to the fringe spacing. In this way, signal-beam phase changes are converted to amplitude changes detected by the photomultiplier.

A complication arises from the fact that the signal-beam amplitude decreases during subtraction. This will cause the photomultiplier output to change even if the phase of the subtracted beam is stable. To avoid this

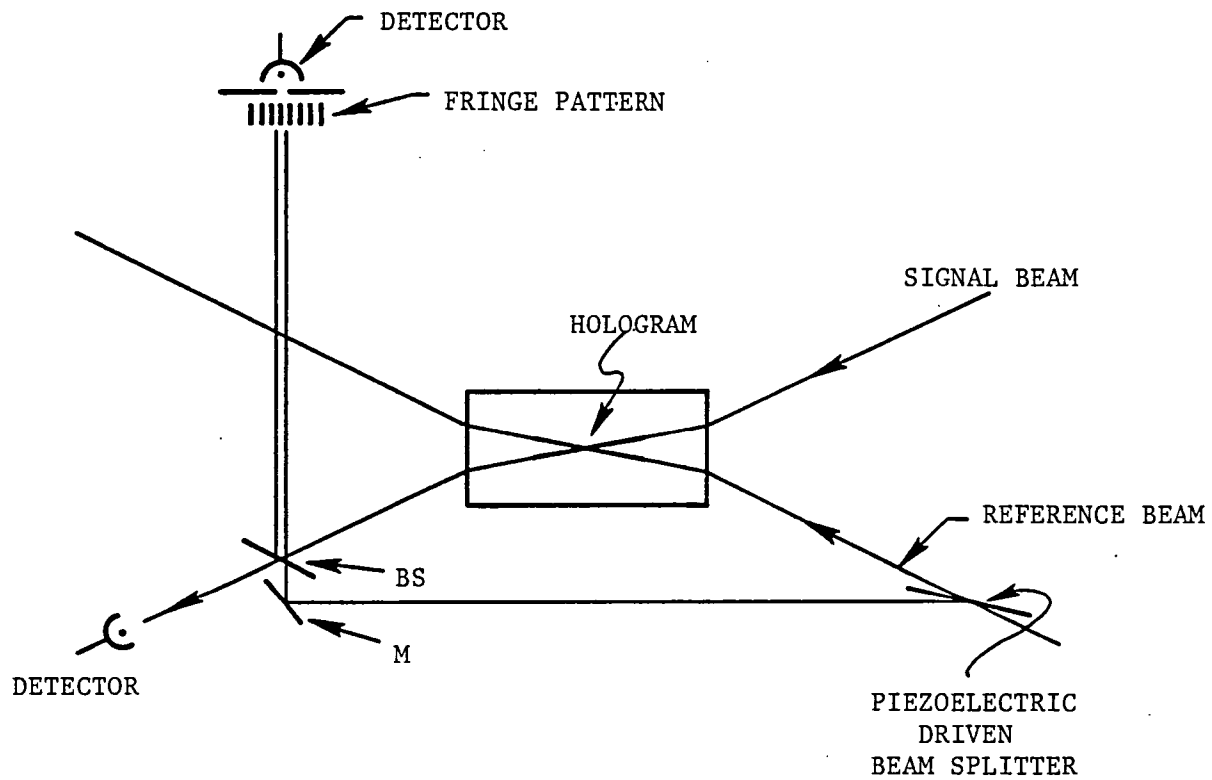


FIGURE III-3. EXPERIMENTAL CONFIGURATION FOR TRACKING THE PHASE OF SIGNAL BEAM DURING HOLOGRAM RECORDING.

complication, a piezoelectrically-translated beam-splitter is used to provide the reference beam component to be mixed with the signal beam in this experiment. The position of the beam splitter is adjusted to keep a dark fringe (or bright fringe) centered on the detector. At any time, the voltage applied to the piezoelectric drive to move the beam splitter the required amount is proportional to the accumulated signal-beam phase change.

A feedback electrical system for tracking the moving fringe pattern could no doubt be devised, but for our preliminary investigation, manual tracking was acceptable. Details of the experiment results are discussed in Sec. IV.

#### SAMPLE-PREPARATION TECHNIQUES

Two types of  $\text{LiNbO}_3$  waveguides were used for the investigations of this program. These were Ti-indiffused waveguides<sup>(23)</sup> and  $\text{Li}_2\text{O}$  outdiffused waveguides.<sup>(24)</sup> The Ti-diffused waveguides have grown more popular for applications in recent years, owing to the ease with which channel waveguides can be formed using standard lithographic techniques<sup>(25)</sup>, owing to the confinement of light closer to the waveguide surface, and owing to the existence of TM modes and modes that propagate parallel to the optical axis of the  $\text{LiNbO}_3$  crystal.<sup>(26)</sup> These are all features absent in outdiffused waveguides, resulting in somewhat restricted use of these waveguides in application-oriented programs. While we performed several experiments with Ti-diffused waveguides, the results generally showed oscillatory behavior with an overall trend toward holographic self-addition rather than self-subtraction. Consequently, we did not pursue this waveguide variety in detail. Our feeling was that diffused Ti was participating in the photo-refractive process in ways too complicated to effectively analyze using the results of the limited set of experiments we were performing.<sup>(27,28)</sup> We emphasized outdiffused samples in the program primarily because they were the ones that best exhibited the self-subtraction phenomena of interest. Understanding the self-subtraction process in these samples was perceived to be the appropriate first step in understanding the process in waveguides generally.

Those wishing to repeat our experiments may note the waveguide-fabrication methods employed. Ti diffused waveguides are formed by e-beam evaporation of about 200 Å Ti on the LiNbO<sub>3</sub> substrate surface and subsequent diffusion of the metal into the substrate at 950° or 1000° C for about 3 h. During the diffusion, O<sub>2</sub> gas is passed over the sample. After diffusion the sample is quenched to about 600° C in an interval of approximately 15 sec. It is then allowed to cool to room temperature at its natural rate or at an accelerated rate requiring as little as 30 min. Usually O<sub>2</sub> gas remains flowing over the sample during the cool down. Although the flowing gas has no effect on waveguide characteristics at temperatures of 600° C or less, it can have significant effect on the photorefractive characteristics of a sample. We have demonstrated this by subjecting waveguides to reducing treatments in Ar and oxidizing treatments in flowing O<sub>2</sub> at temperatures up to 600° C and for times up to 5 h.

The motive for conducting these heat treatments is discussed in Ref. 8. A reducing heat treatment is believed to add electrons to Fe<sup>3+</sup> iron traps in the LiNbO<sub>3</sub>, thus converting them to Fe<sup>2+</sup> donors. This increases the photorefractive sensitivity of the crystal at the same time it decreases the supply of available Fe<sup>3+</sup> electron traps. In the simplest model, the mean free path L of the photo-excited electron varies inversely with the number of available traps. We thus have a mechanism by which a reducing thermal treatment can increase L. According to the theory of Sec. II,  $L/\lambda \gg 1$  is a condition desired for the best self-subtraction. We thus expect a reducing heat treatment in flowing Ar to improve a sample's self-subtraction characteristics. A counter line of reasoning is used to show that an oxidizing thermal treatment can reduce L and hence degrade a sample's capacity for self-subtraction.

Although we employed a number of oxidizing and reducing thermal treatments on several LiNbO<sub>3</sub> waveguides, in only one case were we successful in improving self-subtraction performance. In general our results were not consistent enough to permit the identification of trends to use for guidance in specifying sample preparation methods. The details of particular experiments, however, are provided in the following section.

#### IV. RESULTS OF EXPERIMENTAL STUDIES OF SELF-SUBTRACTION

This section contains the principal experimental results of the program. Approximately 50% of the work was done on a particular outdiffused waveguide sample, #96, which exhibited the best self-subtraction of any sample studied. We begin the section by describing our detailed results with this waveguide, including its history, its potential for self-subtraction data processing, the effects of various experimental configurations on performance, and effects of various heat treatments on performance. Then we will compare our results with sample #96 to results obtained using similarly fabricated samples to show the extent of reproducibility and predictability of self-subtraction phenomena. We will briefly describe the nature of our results with a Ti-indiffused  $\text{LiNbO}_3$  waveguide, and we will close by relating our experimental results to the theoretical predictions of Sec. II.

##### EXPERIMENTAL STUDIES OF SELF-SUBTRACTION IN OUTDIFFUSED WAVEGUIDE SAMPLE #96

Sample #96, purchased "off the shelf" from Crystal Technology, is a 25.4 mm x 12.7 mm x 1 mm y-cut slab that was probably intended for acoustic applications. The polish was inferior to the optical quality polish we receive on specially-prescribed crystals for integrated optical applications. In spite of those unpromising origins, #96 exhibited the best self-subtraction of any sample we studied. The waveguide was made by thermal outdiffusion at 950° C for 1 h in flowing  $\text{O}_2$ . The sample was quenched to 600° C and then allowed to cool slowly to room temperature, probably in flowing  $\text{O}_2$  at all times.

The first hologram recorded in the sample revealed a slow, oscillatory signal-intensity-vs-time curve that tended slowly toward the null associated with self-subtraction. A second run with a reference-to-signal beam ratio of 7.5/1 (down from 33/1) showed a barely noticeable oscillation, and the time required for the signal-beam intensity to fall to 1/e of its initial value was about 320 sec. Following these runs, the sample

was subjected to a 2h anneal in flowing Ar at 500° C to see if any improvement in self-subtraction performance could be obtained.<sup>(8)</sup> In fact, the oscillatory characteristics returned stronger than previously. However, after six days of sample inactivity, a series of new runs were made that showed little or no oscillation and good quality self-subtraction. These runs are the subject of the following subsection.

#### Tests of Sample #96 as a Self-Subtraction Processor

We made a series of measurements with sample #96 in which the crystal performed the operations expected of a self-subtraction processor. That is, repeated self-subtraction holograms were formed after the application of repeated phase shifts and optical erasures. Performance was characterized by measurements of (1) the time constant for subtraction, (2) the contrast ratio, indicating the extent of subtraction attained, (3) the stability of a self-subtraction hologram over long periods of constant writing and read-out, and (4) the reproducibility of the subtraction phenomena after multiple optical erasures and phase shifts.

Most of the results to be described were obtained during the course of one week of investigation. The activities of that week are summarized by Table IV-1. In the context of the table, "erase" means optical erasure with the signal beam blocked. "Rewrite" means writing a new self-subtraction hologram on top of an old one following the application of a phase shift to one of the writing beams. "Erase? (Tesla)" means that a Tesla coil was used to attempt erasure of a waveguide hologram. We did not attempt to verify that the hologram was erased, but we did notice an increase in recording sensitivity after the experiment that could possibly have resulted from the electron bombardment of the surface.

#### Time Constants, Contrast Ratios, and Reproducibility of Self-Subtraction Holograms

Figure IV-1 shows the formation of the self-subtraction hologram associated with the second rewrite of day 7, immediately following an applied

TABLE IV-1. SELF-SUBTRACTION EXPERIMENTAL ACTIVITY USING  $\text{LiNbO}_3$   
OUTDIFFUSED WAVEGUIDE SAMPLE #96

Day	1	2	3	4 and 5	6	7	8
Activity	Write	Erase	Write	Inactive	Rewrite	Rewrite (? - shift)	Erase
	Erase	Write	Erase		Erase	Rewrite ( $\pi$ - shift)	Write
	Write	Erase	Write		Write	Rewrite ( $\pi/4$ - shift)	
			Erase? (Tesla)			Rewrite ( $\pi$ - shift)	
			Write			Rewrite (= Beam Intensities)	

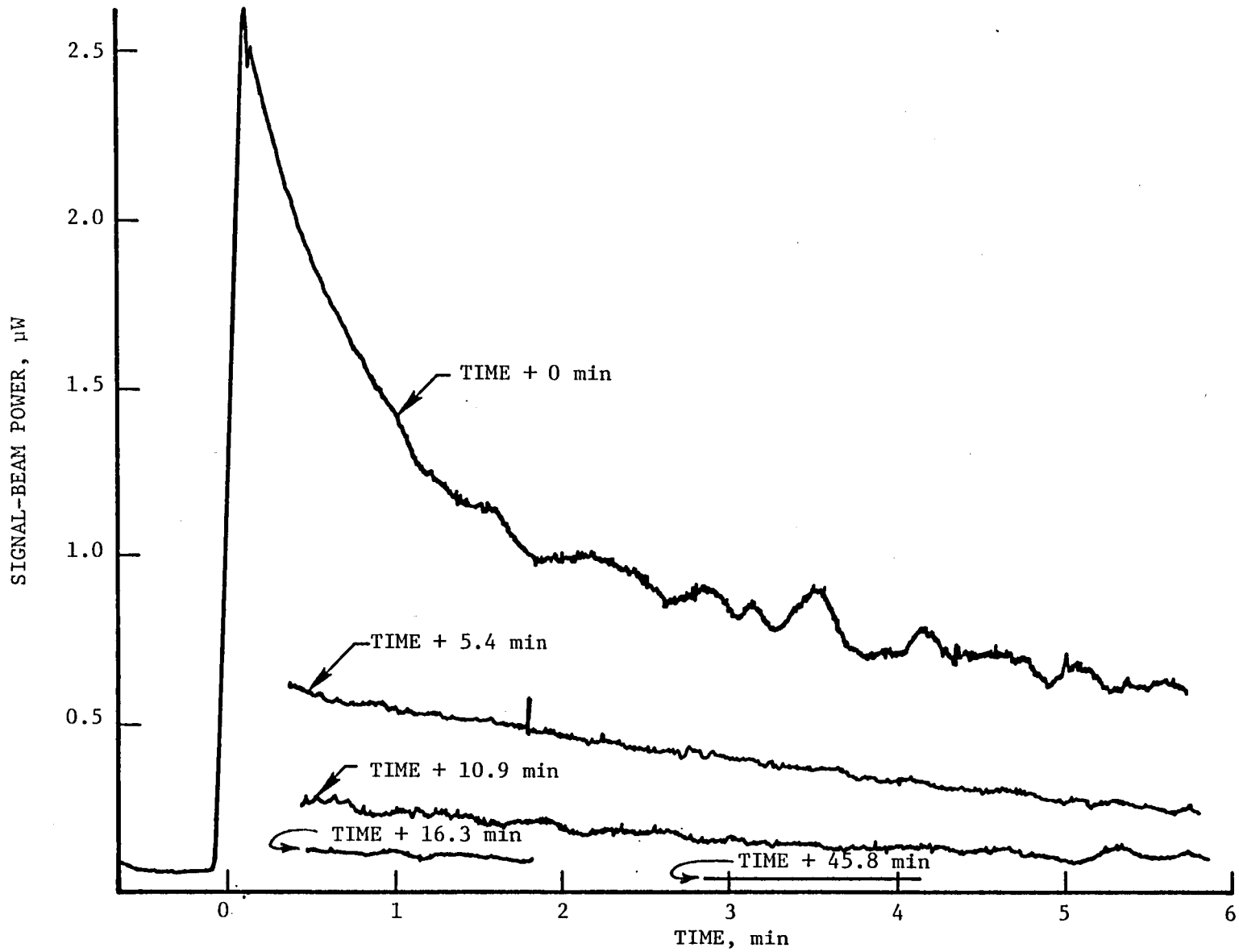


FIGURE IV-1. POWER-VS-TIME FOR A SUBTRACTED BEAM THAT EXPERIENCES A  $\pi$ -PHASE SHIFT AT  $t = 0$  AND WRITES TO A RENEWED CONDITION OF SELF SUBTRACTION.

phase shift of  $\pi$  to peak the signal-beam intensity. The duration of writing encompassed four successive sweeps of the recorder, with the last sweep interrupted for about 30 min. Just prior to application of the phase shift, the previous hologram had achieved a subtraction level of about 0.06  $\mu\text{W}$ . Immediately after the phase shift the signal beam intensity was 2.6  $\mu\text{W}$ , indicating a contrast ratio for the initial hologram of  $2.6/0.06 = 43.7$ . Based on subsequent experiments, it appears possible that there was background scattering contribution of 0.01  $\mu\text{W}$  to the minimum measured signal of 0.06  $\mu\text{W}$ . In this case the contrast ratio would be as large as  $2.6/0.05 = 52.0$ .

The signal for the rewritten hologram of Fig. IV-1 falls to  $1/e$  of its peak value after 144 sec. The signal is 0.1  $\mu\text{W}$  after 946 sec., and after 50 min. of recording it is reduced to 0.05  $\mu\text{W}$ . As mentioned above, as much as 0.01  $\mu\text{W}$  of this subtracted signal could have been associated with background noise. No tendency toward instability is noted after 50 min. of continuous recording.

Following this experiment a phase shift of about  $\pi/4$  was applied to one of the writing beams, and a third self-subtraction hologram was formed. The writing characteristics for this hologram were similar to those of Fig. IV-1, despite the smaller value of the applied phase shift. The subtracted power was a maximum of 0.06  $\mu\text{W}$ , and no tendency toward instability was noted after more than 30 min recording time. The time constant for recording this hologram was 174 sec., and the contrast ratio at the end of recording was a minimum of 40.0.

Finally another  $\pi$  phase shift was applied and yet a fourth self-subtraction hologram was recorded. The time constant was 139 sec. and the final subtracted power was 0.06  $\mu\text{W}$ , as before. The signal power-versus-time curves for holograms three and four of day seven are shown in Fig. IV-2 and 3, respectively.

These results were obtained with writing beams having unequal intensities in the approximate ratio 14:1. The more intense reference beam was 4 mm wide and the signal beam was 1 mm wide. The power in the output reference beam was 20.8  $\mu\text{W}$ , from which we estimate the waveguide intensity to be on the order of  $0.1\text{W}/\text{cm}^2$ . The external Bragg angle of the hologram was  $14^\circ$ , corresponding to a fringe spacing of 1.3  $\mu\text{m}$ . The beam geometry is that shown in Fig. III-1.

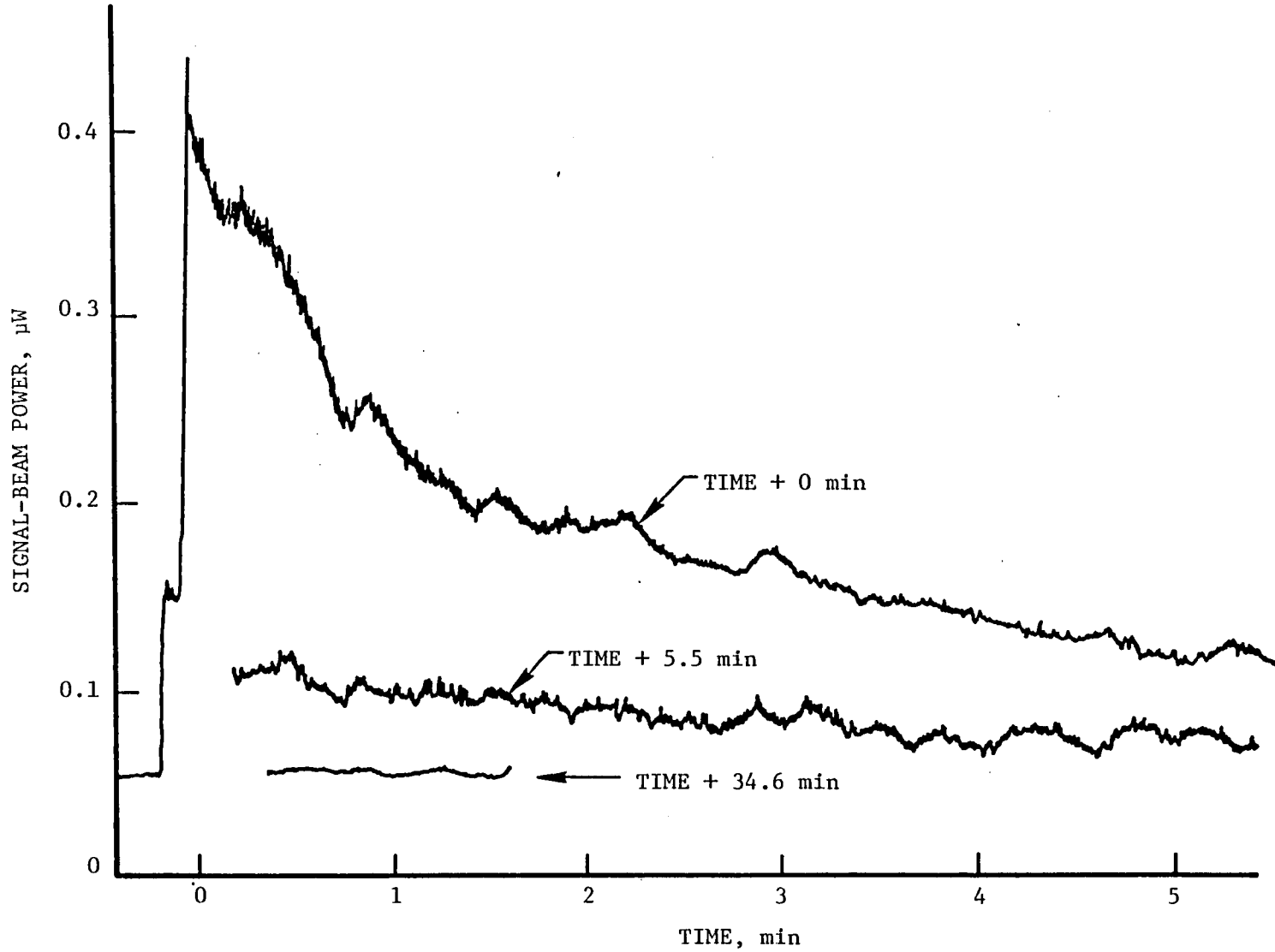


FIGURE IV-2. POWER-VS-TIME FOR A SUBTRACTED BEAM THAT EXPERIENCES A  $\pi/4$  PHASE SHIFT AT  $T = 0$  AND WRITES TO A RENEWED CONDITION OF SELF SUBTRACTION.

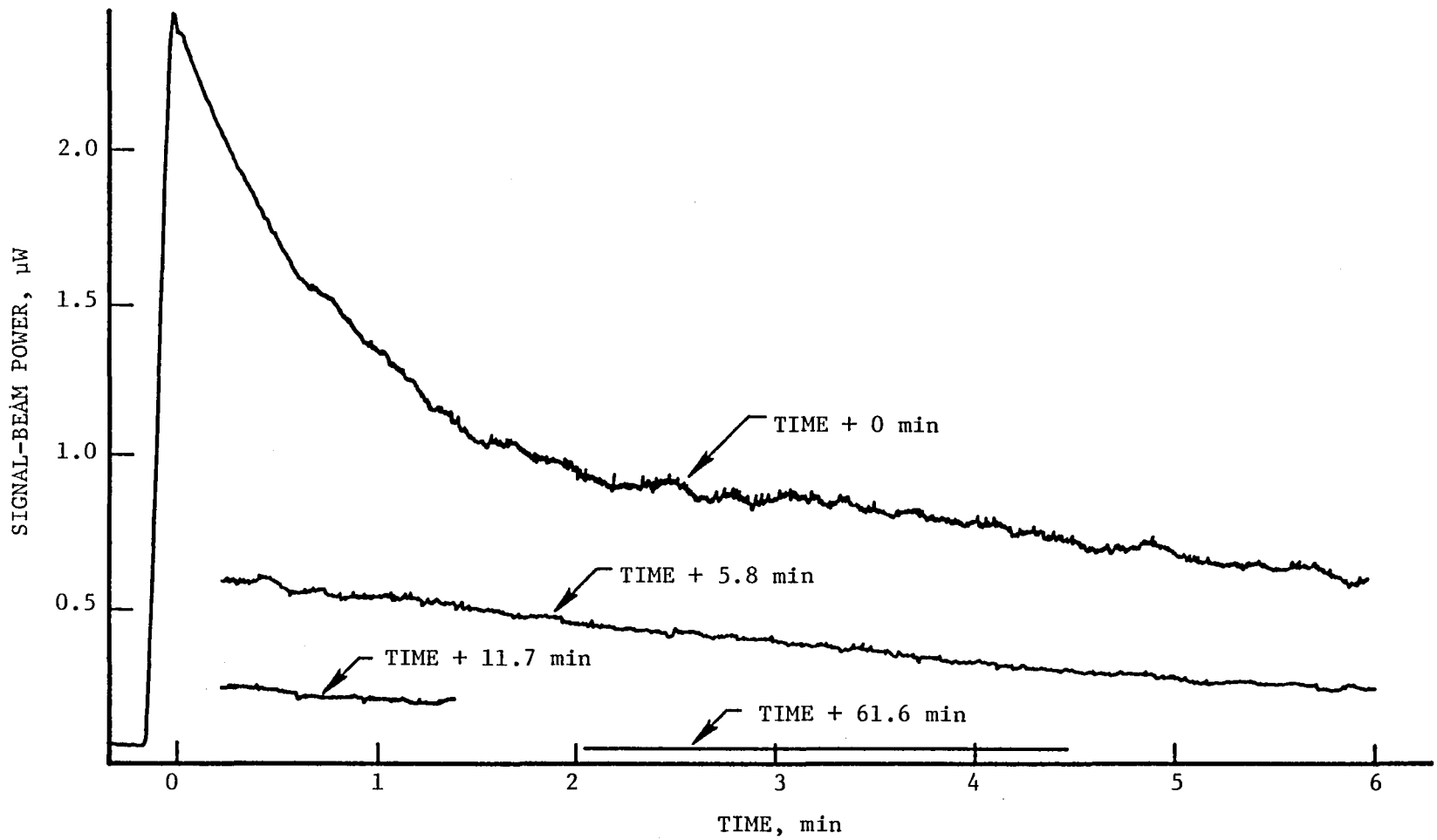


FIGURE IV-3. POWER-VS-TIME FOR A SUBTRACTED BEAM THAT EXPERIENCES A SECOND  $\pi$  PHASE SHIFT AND WRITES TO A RENEWED CONDITION OF SELF SUBTRACTION.

The last hologram recorded on day 7 and the only hologram of day 8 differed from the above holograms in that nearly equal writing beam intensities were employed. A slight tendency toward instability was noted. To be specific, in the final run a contrast ratio close to 57 was reduced to 27 by continued writing at which level stabilization appeared to have been achieved.

Earlier experiments, namely, those occurring on days 1-5 of Table IV-1, differed from later experiments in that equal widths for signal and reference beams were employed. The widths were probably close to 3 mm. The overall area of the hologram is several times larger as a result of the use of two wide beams, and this appears to be associated with a slight reduction in the self-subtraction time constant. With reference and signal beam intensities equal to each other but less than the intensities used in the last runs described above, the time constant was reduced from 140 sec. to about 100 sec. Further reduction occurred with the use of unequal beam intensities. The shortest time constant of about 60 sec was obtained with a 73/1 beam ratio following Tesla-coil exposure of the waveguide surface. We cannot speculate as to whether the large beam ratio or the exposure dominated in producing the reduced time constant, but this is a question worthy of future investigation. Time constants lower than tens of seconds will probably be desirable for most applications.

#### Sensitivity of Self-Subtraction Holograms to Applied Phase Shifts

Figure IV-4 shows the results of an experiment to test the sensitivity of a self-subtraction hologram to applied phase shifts. The hologram is that associated with Fig. IV-3. The initial subtracted intensity is about 0.06  $\mu$ W. At intervals averaging 40 sec. an external phase shift is applied to one of the writing beams and then removed. Each phase shift is larger than the previous one by a certain increment  $\Delta\phi$  which can be determined from the data. We assume that the intensity of the n-th pulse in Fig. IV-4 is described by

$$I_n = I_{bg} + 0.5I_{max} [1 - \cos(\phi_0 + n\Delta\phi)], \quad (IV-1)$$

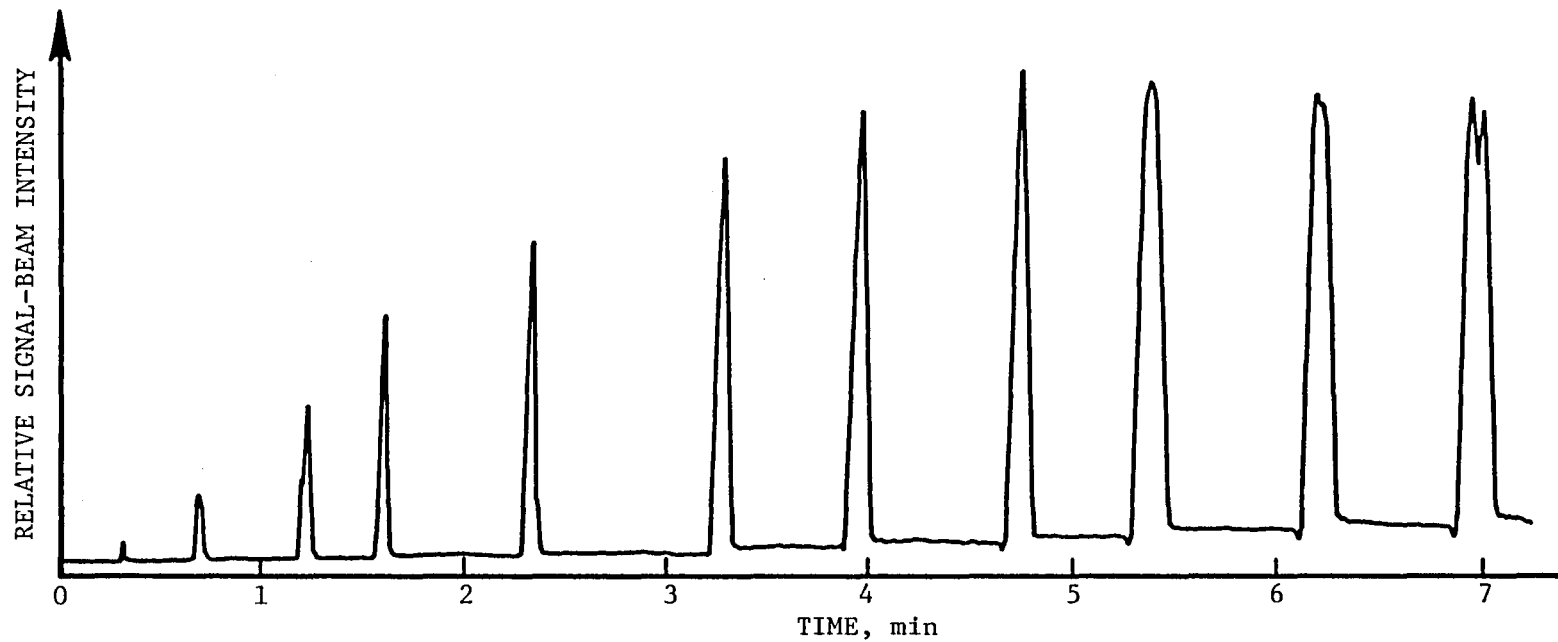


FIGURE IV-4. INTENSITY VS TIME FOR A SUBTRACTED BEAM IN THE PRESENCE OF EXTERNALLY APPLIED PHASE SHIFTS.

where  $I_{bg}$  is the background intensity prior to the phase shift,  $I_{max}$  is the peak signal associated with a  $\pi$  phase shift,  $\phi_0$  is any phase offset associated with the self-subtraction mechanism, and  $\Delta\phi$  is the phase increment.

Figure IV-5 shows a plot of  $(I_n - I_{bg})/I_{max}$  versus the phase index  $n$ . The theoretical fit is obtained using  $\phi_0 = 0$  and  $\Delta\phi = 22^\circ$  in Eq. (1). There is fairly good agreement at lower values of  $n\Delta\phi$ . From Fig. IV-4, note that the first phase shift  $\Delta\phi = 22^\circ$  results in a signal comparable to the background intensity level. We have, therefore  $S/N = 1$  when  $\Delta\phi = 22^\circ$ . This describes the sensitivity of the sample as a phase-shift processor.

Figure IV-5 shows increasing discrepancy between theory and experiment at values of  $n\Delta\phi$  greater than  $180^\circ$ . This may indicate a slight degradation of the hologram caused by the repeated phase shifts. It is interesting to note that following the last phase shift the minimum subtracted signal is observed at  $\phi_0 = 9^\circ$  rather than  $\phi_0 = 0^\circ$ , as is the case initially. That is, an offset in the relative phase required for self-subtraction develops upon repeated applied phase shifts. If one allows the beams to continue writing, however, the intensity at  $\phi_0 = 9^\circ$  increases at first and then falls back to its minimum value where it remains stable.

#### Stability of a Self-Subtraction Hologram to Continuous Seven-Hour Readout.

The experiments summarized by Fig. IV-1,2, and 3 show that self subtraction holograms are stable under continuous readout for times up to 65 min. In applications, self-subtraction processors could very possibly be subjected to continuous readout over a period of months, during which they should remain stable. By use of the word stable we mean to infer that no significant deviations from the minimum subtracted signal occur except those which are triggered by phase shifts in the writing beams.

We investigated the stability of a self-subtraction hologram in sample #96 for a maximum interval of seven hours. Figure IV-6 shows the first 30 min. of hologram recording, during which time a subtracted intensity level of  $0.04 \mu W$  is achieved. Figure IV-7 then shows the subtracted intensity-versus-time variation for the next 6 h 30 min. The average subtracted signal of  $0.03 \mu W$  is stable to within  $\pm 15\%$ . The degree of

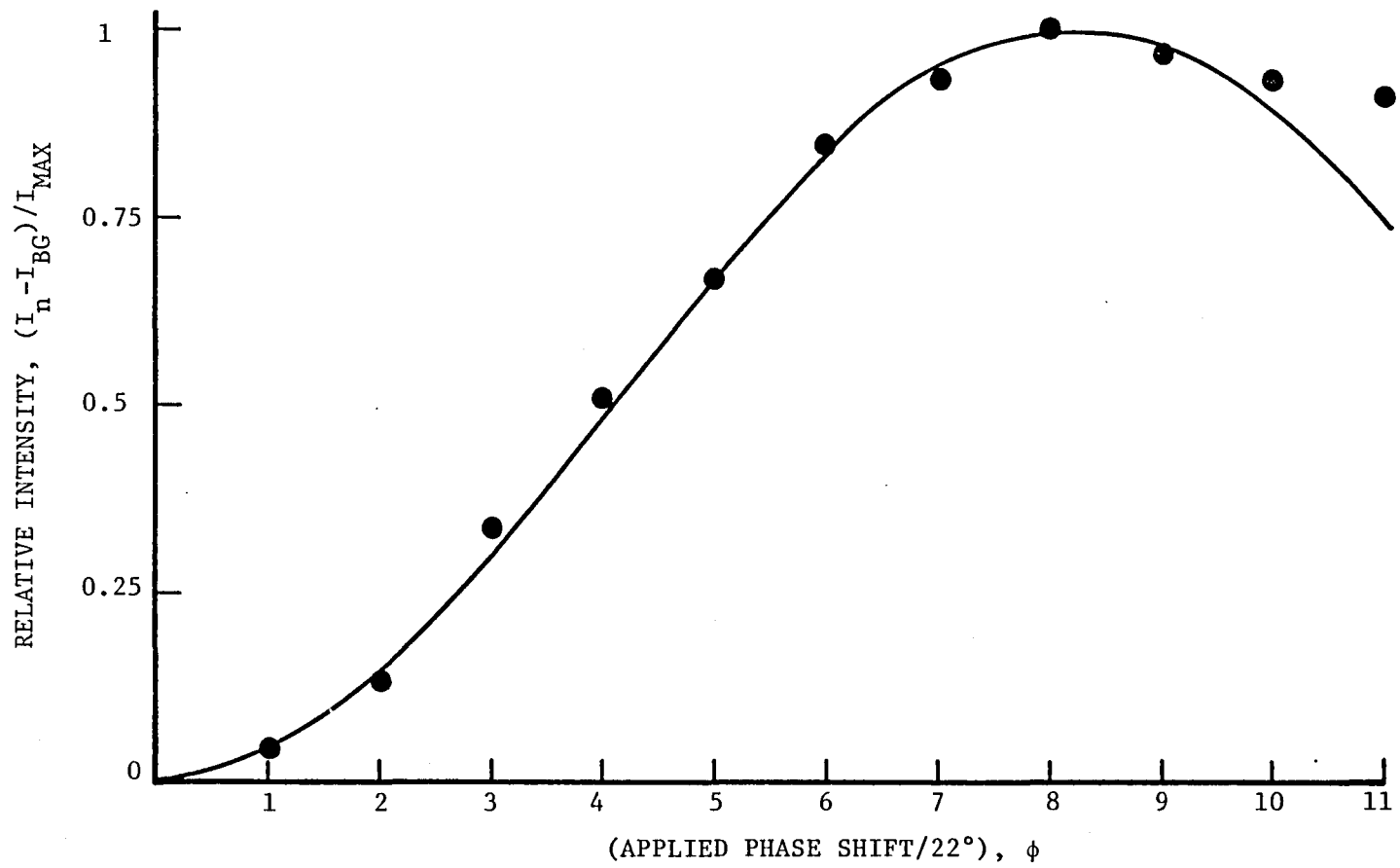


FIGURE IV-5. VARIATION OF SIGNAL BEAM INTENSITY WITH APPLIED PHASE SHIFT.

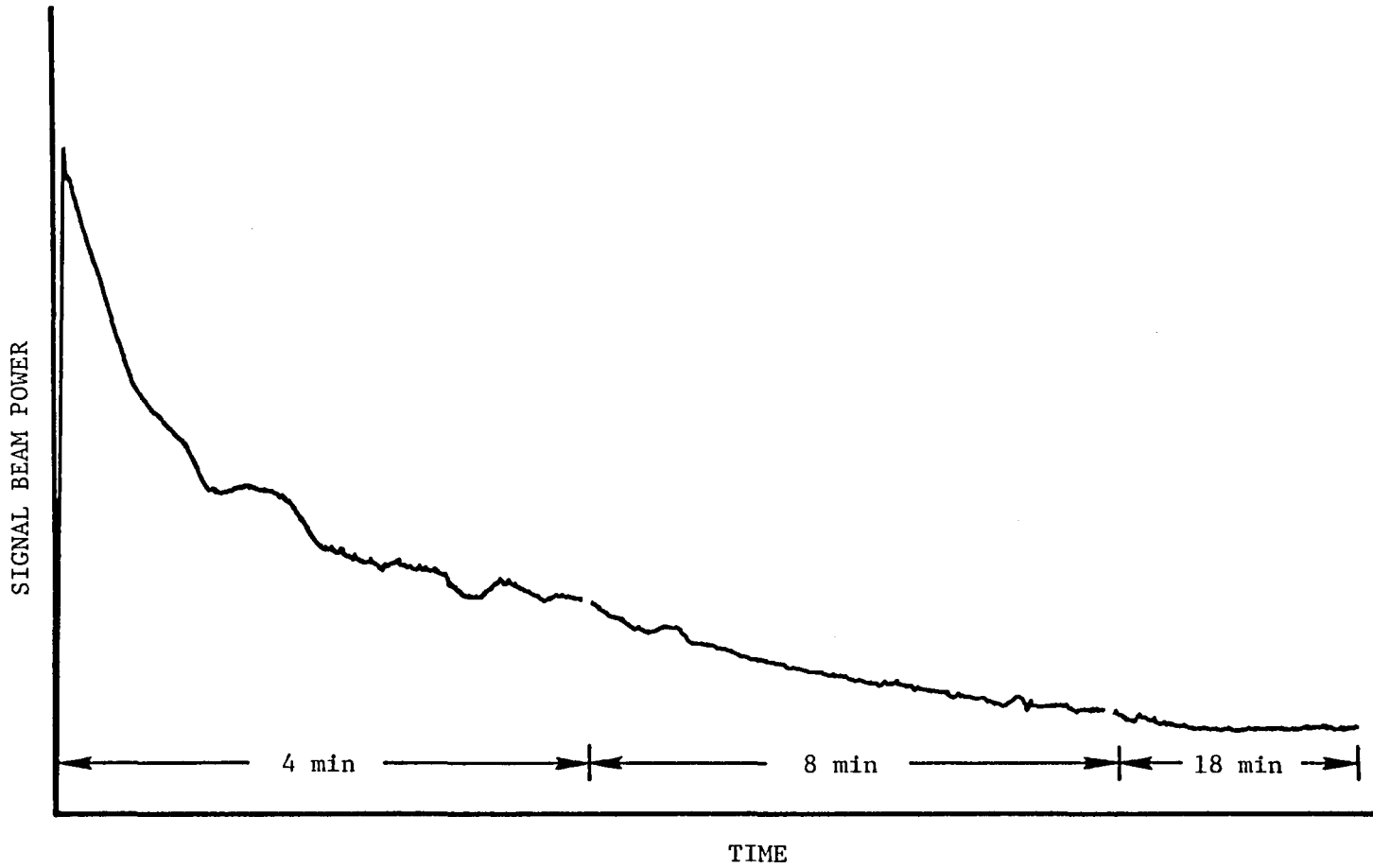


FIGURE IV-6. POWER-VS-TIME CHARACTERISTICS OBSERVED DURING THE FIRST 30 MIN OF A 7 H STABILITY TEST.

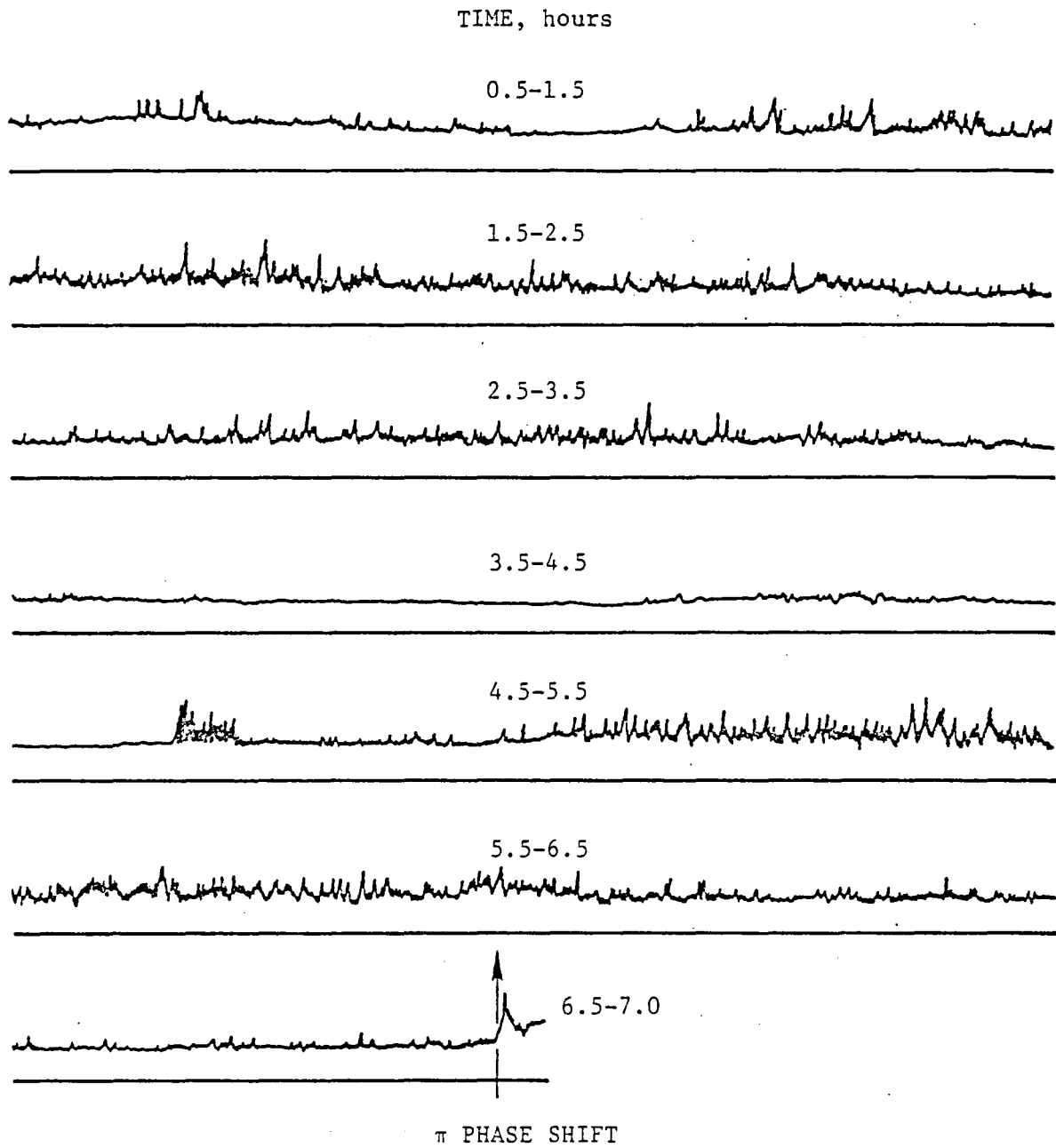


FIGURE IV-7. SUBTRACTED POWER (VERTICAL) VS TIME (HORIZONTAL) IN THE INTERVAL 0.5-7.0 h. AVERAGE SUBTRACTED POWER  $\approx 0.03 \mu\text{W}$ .

fluctuation about the average signal changes in time and is apparently the result of activity in the laboratory, such as people working, or changes in the environment associated with the air-conditioning system. At the end of the run a  $\pi/2$  phase shift was applied and a contrast ratio of 43 measured. This is comparable to the contrast ratio achieved after much shorter runs. The beam ratio used to make this run was 14/1, as measured at the waveguide output. A value 34/1 was measured at the waveguide input. The difference indicates nonuniform coupling of the reference and signal beams. This is not important to the experiment but indicates a large uncertainty as to the correct beam ratio in the waveguide. Other parameters of the experiment were the same as those for the experiments summarized by Figs. IV-1,2, and 3.

#### Sensitivity of Self-Subtraction Holography to Bragg Angle

The results described to this point suggest that self-subtraction characteristics are rather insensitive to parameters such as beam width and beam ratio. We now begin a discussion of parameters to which self-subtraction is fairly sensitive, beginning with the Bragg angle used in recording; that is, the half angle between the two intersecting beams as measured in air.

The motive for studying the dependence of self-subtraction on the Bragg angle,  $\theta_B$ , is the important role played by the quantity  $\tan^{-1} KL$  in the theory of Sec. II, where

$$KL = (4\pi L/\lambda_o) \sin\theta_B, \quad (IV-2)$$

$L$  is the mean free path of conduction electrons and  $\lambda_o$  is the free-space optical wavelength. Values of  $KL$  larger than one are most compatible with good self-subtraction, at least according to the photorefractive model we employed. One can vary  $KL$  by changing the mean path length  $L$  or the magnitude of the grating wavevector,  $K = (4\pi/\lambda_o) \sin\theta_B$ . An easy way to vary the latter parameter is to change the Bragg angle,  $\theta_B$ . Since our initial choice  $\theta_B = 14^\circ$  gave good self subtraction, indicating  $KL \gg 1$ , we thought that 10 X reductions in  $\theta_B$  might be necessary to reduce  $\tan^{-1} KL$  enough to see an effect. However, we found that significant variations in self-subtraction characteristics occurred with only 20% variations in  $\theta_B$ .

We tested five different Bragg angles in the range  $5.5^\circ$  to  $17.9^\circ$ . For  $\theta_B = 17.9^\circ$  and  $13.9^\circ$ , the subtracted beam intensity showed a generally monotonic decrease toward the saturated level. For  $11.1^\circ$ ,  $7.25^\circ$  and  $5.5^\circ$ , a short-lived initial decrease in the subtracted intensity was followed by a large increase (holographic self-addition) and then the subtraction process took over. The variation in intensity as a function of writing time for these experiments is shown in Fig. IV-8. The photorefractive model of Sec. II does not appear to provide a basis for interpreting these results.

#### Sensitivity of Self-Subtraction Holography to Thermal Oxidizing and Reducing Treatments.

The variation of  $\theta_B$  was used, as described above, to accomplish a variation in the photorefractive parameter  $KL$  of Eq. 2 by causing a change in  $K$ . Oxidizing and reducing heat treatments can change the product  $KL$  through their effect on the electron path length  $L$ . We therefore were motivated to study the variations in self-subtraction caused by oxidizing and reducing thermal treatment of sample #96 and other samples in oxygen and argon, respectively. The details of these thermal treatments were described in Sec. III.

In this section we have already indicated that a reducing treatment performed on waveguide #96 after it was fabricated helped to improve its self-subtraction characteristics. We now describe the results of other thermal treatments on #96 that took place in the time frame 4.5 - 5.0 months after the last experiments described above, those summarized by Fig. IV-8. The photorefractive properties of the sample do not appear to have degraded over the 4.5 month delay between experiments. However, a 5 h heat treatment in flowing Ar at  $600^\circ$  C was found to cause a serious impairment in the self-subtraction characteristics of the sample. With a Bragg angle of  $18^\circ$ , the initial reduction of signal beam intensity with recording time progressed at a rate slower than previously and reversed itself before 50% of the initial signal level was reached. No subsequent tendency toward subtraction was observed during the observation time, which was approximately twice the time that the initial signal intensity decreased. In several runs the final

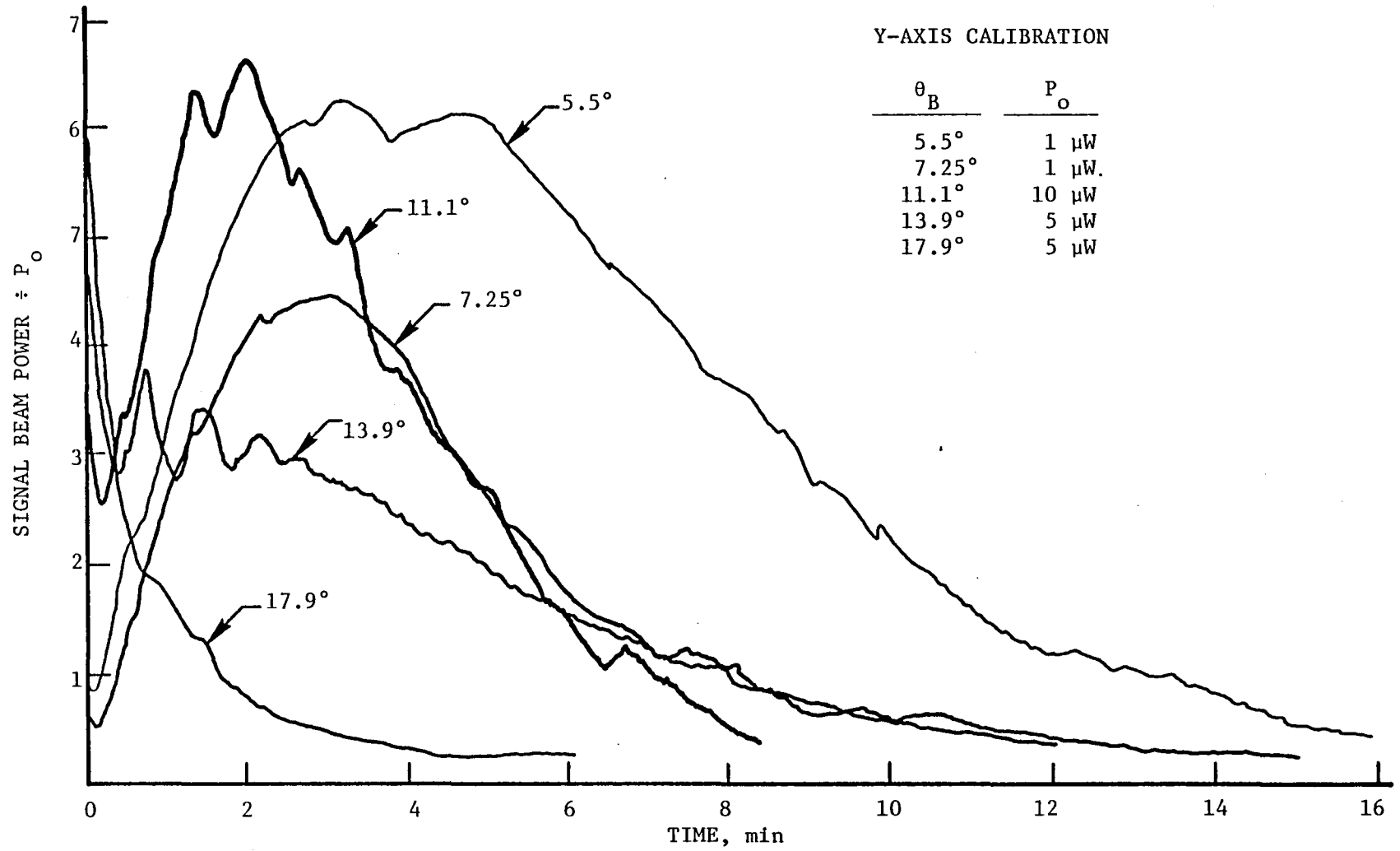


FIGURE IV-8. SELF-SUBTRACTION CHARACTERISTICS OF HOLOGRAMS IN OUTDIFFUSED  $\text{LiNbO}_3$  WAVEGUIDE #96, MEASURED FOR FIVE DIFFERENT BRAGG ANGLES.

intensity observed was greater than the initial intensity (holographic self addition). It is possible that this situation would have reversed if we had taken data for a long enough period. Figure IV-8 provides evidence for this possibility. However, the time required would have been so great as to render the sample useless as a self-subtraction processor, so we did not continue the measurement.

When a second heat treatment of 5 h in flowing Ar at 600° C was given to sample #96, the self-subtraction characteristics of the sample did not appear to change significantly from the degraded characteristics observed following the first reducing heat treatment. As described in Sec. III, it was anticipated that these reducing heat treatments would have a beneficial effect on self-subtraction by converting Fe<sup>3+</sup> traps to Fe<sup>2+</sup> donors, thus increasing both photorefractive sensitivity and path length. Apparently this simple-minded viewpoint is not sufficient to describe the actual dynamics of the photorefractive process. Subsequently, we provided sample #96 with an oxidizing heat treatment to see if we could reverse the self-subtraction degradation caused by the two reducing heat treatments. The oxidation was carried out over a period of 4 h, with the sample maintained in flowing O<sub>2</sub> at 600° C. The effect of this treatment was, if anything, to reduce the exchange of energy between writing beams. No tendency toward either self subtraction or self addition was observed.

Our final experiment with sample #96 was to reproduce the conditions used in making the initial waveguide; that is, the sample was heated in flowing O<sub>2</sub> at 950° C. The length of the heat treatment was 1/2 h, in contrast to the 1 h treatment used to make the initial waveguide. The sample was preheated in O<sub>2</sub> at 600° C for 2.75 h prior to raising the temperature to 950° C. At the end of the heat treatment the sample was rapidly cooled to 600° C and then brought to room temperature over a period of 1/2 h. Oxygen gas remained flowing over the sample throughout the process. Only one self-subtraction run for the sample was performed following this treatment and that run indicated little or no tendency toward self-subtraction.

In summary, a variety of thermal treatments were performed on sample #96. A 2 h reduction in flowing Ar at 500° C was performed after the outdiffused waveguide was fabricated, and this was the only beneficial

heat treatment from the point of view of optimizing self-subtraction. Even in this case, beneficial effects appeared only after a 6 day time delay, and it is possible that the thermal treatment had little to do with their appearance.

Although the good self-subtraction characteristics of sample #96 remained in force for 4.5 months, the first subsequent thermal anneal at 600° C removed them, and no thermal anneal attempted thereafter was able to restore them. In fact, no significant trends were observed following successive oxidizing or reducing treatments. As a result we can not confidently predict the most suitable fabrication method for a waveguide to be used for self-subtraction, nor can we state the optimum self-subtraction performance to be expected from  $\text{LiNbO}_3$  waveguides. However, we did work with other waveguide samples than #96, and these tended to show fair self-subtraction in their as-fabricated state when they were fabricated by methods similar to those used for sample #96. This provides us with a starting point for any future research that may be undertaken on self-subtraction. It is suggested that thermal heat treatments of shorter duration and lower temperatures be employed to insure that dramatic changes in self-subtraction performance are avoided. In this way, trends may be identified and an optimized set of fabrication conditions may result. In the following subsection we present, for guidance, the results of our experiments on samples other than #96.

#### EXPERIMENTAL STUDIES OF SELF-SUBTRACTION IN OUTDIFFUSED WAVEGUIDE SAMPLES #97, 100, AND 162

##### Performance of Sample #97

Sample #97 was outdiffused using the same procedure employed for sample #96; namely, a 950° C anneal in flowing  $\text{O}_2$  for 1 h, followed by a rapid quench to 600° C and a slow cool to room temperature. The light anneal in Ar that was applied to #96 after its fabrication was not applied to #97. Perhaps as a result, the performance of #97 never matched the best performance of #96. Instead, #97 behaved qualitatively similar to the way #96

behaved in the as-fabricated state, showing slow subtraction with a tendency toward oscillation or instability. Self-subtraction characteristics apparently did not benefit from a 6.6 month delay between fabrication and testing.

The ratio of initial signal-beam intensity to reference beam intensity that gave the best subtraction was 1/10. In this case the self-subtraction time constant was about 10 min. However, there appeared to be a tendency toward instability since the signal-beam intensity was climbing slowly when the run was terminated at 27 min. In the case of 1/1 or 1/100 beam ratios, the steady-state trend seemed to be toward a constant, unsubtracted signal beam. We recall that sample #96 did not show a similar dependence of subtraction capability on the beam ratio.

Following these initial measurements, sample #97 was subjected to two 5 h heat treatments in Ar at 600° C. These did not result in any significant change in the self-subtraction characteristics of the sample. However, a third heat treatment, in flowing oxygen at 600° C for 4 h, resulted in the very dramatic changes shown in Fig. IV-9. The signal beam intensity-vs-time characteristic is quasi-periodic. Deviations from exact periodicity are fairly regular. Unfortunately, the physical changes in the crystal that served to produce this interesting effect remain hidden from view. It would, in the future, be useful to perform a detailed analysis of the theory of Sec. II to see if effects like those observed here can be explained using the simple photorefractive model on which that theory is based. Ultimately, it will be desirable to experimentally characterize the oxidation-reduction state of the crystalline impurities to obtain more information about the source of behavior like that shown in Fig. IV-9.

#### Performance of Sample #100

Sample #100 was an outdiffused  $\text{LiNbO}_3$  waveguide formed in "off the shelf" material similar to samples #96 and 97. The outdiffusion heat treatment, however, was carried out very differently. The sample was heated to 1100° C, at which point the oven was turned off. The time spent in going from 950° C to 1100° C was 7 min., and the time spent in cooling to 950° C

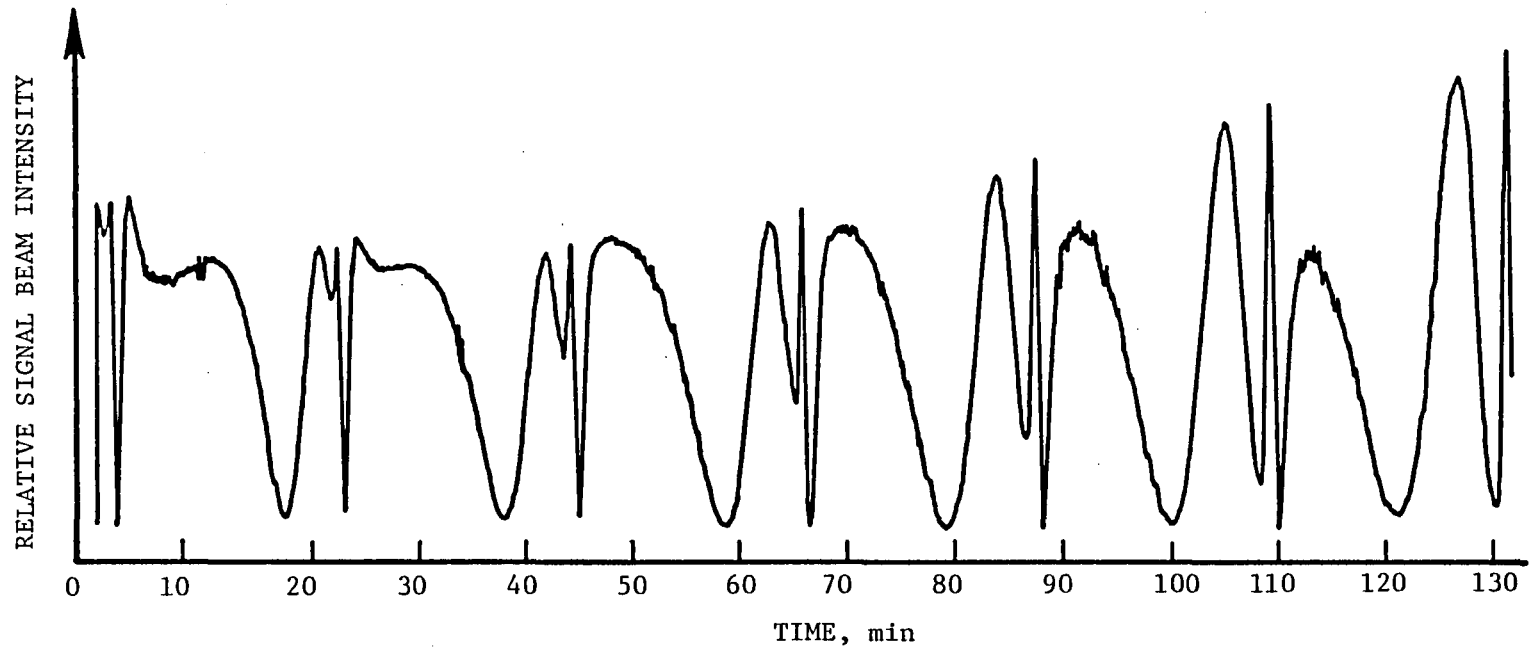


FIGURE IV-9. SIGNAL-BEAM INTENSITY VS TIME FOR SAMPLE #97  
FOLLOWING AN OXIDIZING THERMAL TREATMENT.

again was 6 min. The waveguide expected to result from this procedure is shallower than the conventional outdiffused waveguide.<sup>(29)</sup> Consequently, its photorefractive properties should be more sensitive to the oxidation-reduction state of impurities at the waveguide surface.

Several runs were made using this sample. One run was made using the waveguide as fabricated; another was made after a four hour oxidation carried out at 600° C. The most notable feature of the signal-intensity-vs-time characteristics of holograms formed in this waveguide was their lack of consistency. In some runs the signal intensity decreased in time as expected for self-subtraction. When it did so, however, two time constants were in evidence for different runs: one on the order of minutes, the other on the order of hours. In other hologram-formation experiments, the signal-intensity versus time curve showed oscillatory behavior with a characteristic period on the order of 20 min. The oscillations were not, however, periodic or quasi-periodic like those of Fig. IV-9.

Because of these inconsistent and unexplicable results, we ceased experimenting with sample #100. One conclusion that may be drawn from the work is that the waveguide fabrication treatment employed for the sample was not conducive to good self-subtraction.

#### Performance of Sample #162

Sample #162 differed from previously discussed samples in that it was special-ordered for integrated-optics applications. The 25 x 25 x 3 mm<sup>3</sup> substrate was sawed into two similar 12 x 25 x 3 mm<sup>3</sup> substrates, designated 162A and 162B. The former was subjected to a 1 h outdiffusion treatment similar to that used for the preparation of #96 and #97. The latter was subjected to a 30 min. outdiffusion to see what effects, if any, might be associated with the time of the thermal treatment, other factors remaining constant.

Most experimental data were taken using sample #162A over a period of two weeks. Although the range of experiments performed was not as exhaustive as with sample #96, sample 162A appeared to come close to matching the performance level of #96. For example, self-subtraction holograms were

repeatedly written following the application of  $\pi$  phase shifts. The time constants for reaching the subtracted condition were typically 2 min. Contrast ratios were not measured but appeared to be comparable to those obtained using sample #96.

What is most interesting about sample #162A is that its performance as a self-subtraction waveguide improved after the first three days of experimentation with it. During these days the sample exhibited self-subtraction, but an occasional tendency of the signal beam to oscillate in intensity rather than to subtract was observed. This tendency vanished in experiments performed about one week following initial experiments with the sample. A similar delay in the onset of good self-subtraction performance was also observed in sample #96, though in this case an intervening thermal reduction treatment could have had some effect. The possibility is that optical preconditioning of the sample is necessary to produce good self-subtraction characteristics. Other samples tested in the program were not evaluated over the course of a week, at least without complicating intervening thermal treatments. Consequently, any beneficial effects of optical preconditioning were not observed.

Sample #162B, similar to #162A except for a shorter waveguide fabrication time, was tested only over a two day span. It was not found to exhibit good self-subtraction, even when compared to the initial results for #162A. The lesson seems to be that shorter outdiffusion times are not helpful for forming waveguides with good self-subtraction characteristics.

Fig. IV-10 shows the results of experiments performed using sample #162A in which a sequence of five abrupt phase shifts is applied to one of the recording beams. Following each phase shift, the signal-beam intensity (lower curve in the figure) begins to decrease as required for self-subtraction. Also shown in the figure is the reference beam intensity (upper curve) which increases as the signal-beam intensity decreases (holographic self addition). This is in accord with the requirement that optical energy be conserved between the two writing beams. In Fig. IV-10 the vertical scales for the reference and signal-beams are not identical. Consequently the different amplitudes for the two beams are not in violation of the energy-conservation requirement.

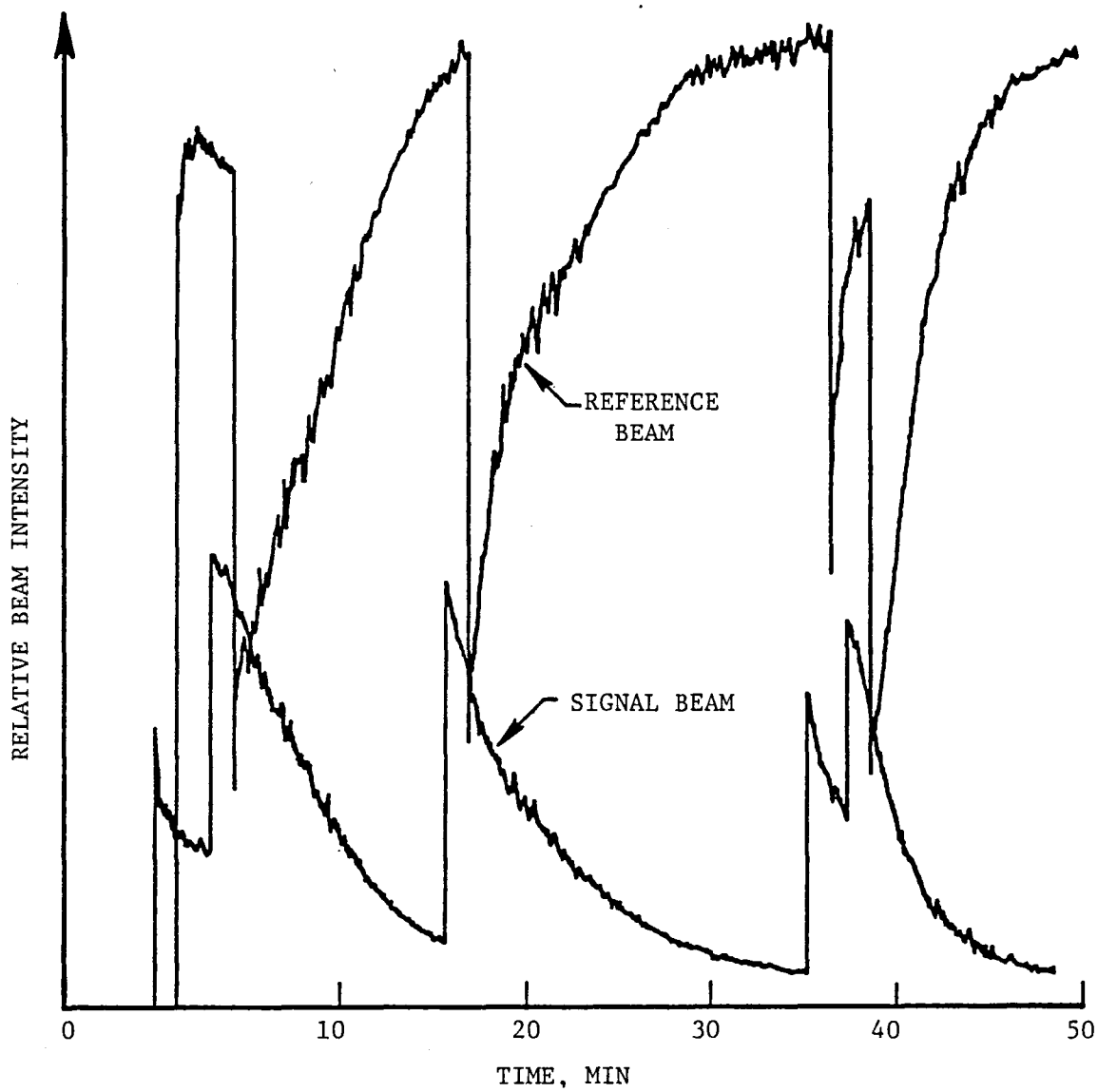


FIGURE IV-10. TEMPORAL VARIATION OF SIGNAL AND REFERENCE-BEAM INTENSITY IN THE PRESENCE OF FIVE APPLIED PHASE SHIFTS.

EXPERIMENTAL STUDIES OF SELF-SUBTRACTION IN  
Ti-INDIFFUSED WAVEGUIDE SAMPLE #135

Waveguides formed in  $\text{LiNbO}_3$  by the thermal diffusion of oxidized Ti films are commonly used in integrated optic applications. (23,25-28) Two good reasons for this are (1) the relative ease with which channel waveguide structures are formed using photolithography and (2) the confinement of the light close to the waveguide surface where it can be more readily switched or modulated by acoustic and electric perturbations. For holographic applications, however, the Ti dopant adds a degree of complexity because it acts as an impurity in altering the photorefractive properties of the waveguide. (27,28)

The  $\text{Ti:LiNbO}_3$  waveguide that we studied in most detail was formed by the thermal diffusion of a 270Å Ti film at  $950^\circ\text{C}$  for 3 h flowing  $\text{O}_2$ . We looked for self-subtraction phenomena at Bragg angles of  $5.5^\circ$  and  $20.6^\circ$ . We took data for both positive and negative c-axis orientations to insure that the proper conditions for self-subtraction were achieved at least part of the time. Nevertheless, at a  $5.5^\circ$  Bragg angle, holographic self-addition was encountered for both c-axis orientations. In each case, the weaker of two beams used to write the grating was amplified until a saturation intensity was reached. The saturation intensity was 32 times the initial intensity in one case, and 9.6 times the initial intensity in the other.

When a Bragg angle of  $20.6^\circ$  was employed, we observed that the intensity of the weaker of the two writing beams oscillated in time. For one c-axis orientation, successive oscillations appeared to be damped. For the other orientation successive oscillations were as shown in Fig. IV-11. The quasi-periodic nature of the oscillations, with increasing amplitude and period, is reminiscent of the results obtained with outdiffused waveguide #97, shown in Fig. IV-9.

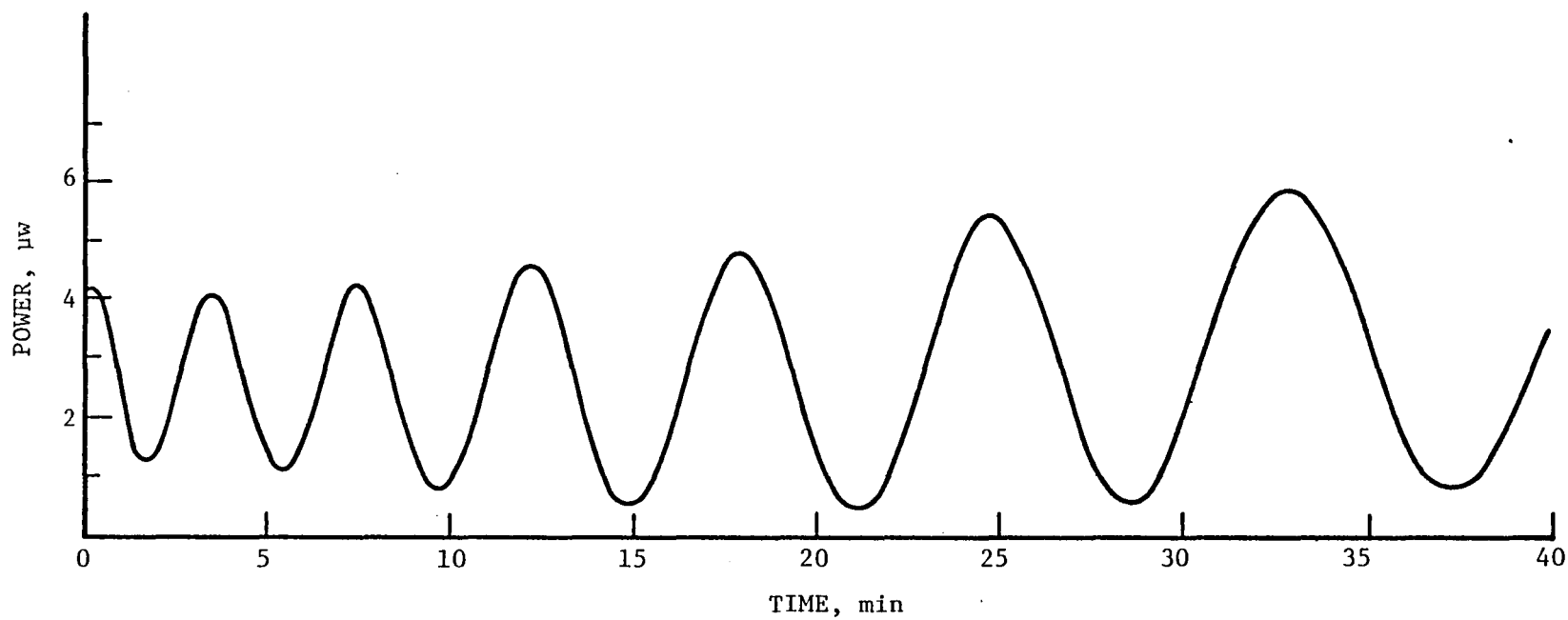


FIGURE IV-11. OSCILLATING OUTPUT POWER FOR THE WEAKER OF TWO BEAMS USED TO WRITE A HOLOGRAM IN A  $\text{Ti:LiNbO}_3$  WAVEGUIDE.

## COMPARISON OF THEORY AND EXPERIMENT

### Subtracted-Beam Intensity Versus Time

We have previously indicated that the theory for self-subtraction presented in Sec. II has not been exercised enough for us to learn all of its ramifications. We do not know, for example, if the theory can describe the quasi-periodic oscillations of Figs. IV-9 and IV-11. In so far as the theory has been exercised, it predicts that self-subtraction does exist for a certain reasonable photorefractive model. This is consistent with the fact that we experimentally observe self-subtraction, except that our observations show an exponential-like decay to the subtracted state whereas the theory predicts a damped-oscillatory decay. Apparently, some feature has been left out of the physical model which might account for the observed smoothing of the subtraction curve. Only in one experiment did we observe a damped oscillatory approach to the subtracted state. This result, shown in Fig. IV-12, was obtained using sample #162A. It was not reproduced in subsequent experiments with that sample.

### Subtracted-Beam Phase Versus Time

A measurement of subtracted intensity as a function of time, such as that shown in Fig. IV-12, conveys no information about the phase of the subtracted beam. A measurement of the phase as a function of time therefore provides a second means of comparison of theory and experiment, one which we explored at the close of the program.

The theoretical results of Fig. II-6 and II-7 shows that the phase of the subtracted beam is relatively constant except at times when the subtracted intensity is near a minimum. Our thought was that a sequence of rapid phase variations might occur in our experiments even though, for one reason or another, local minima in the subtracted beam intensity were washed out.

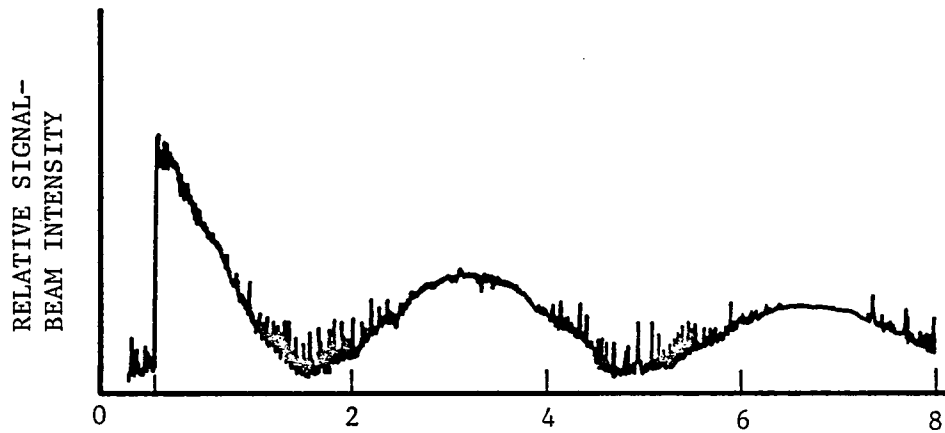
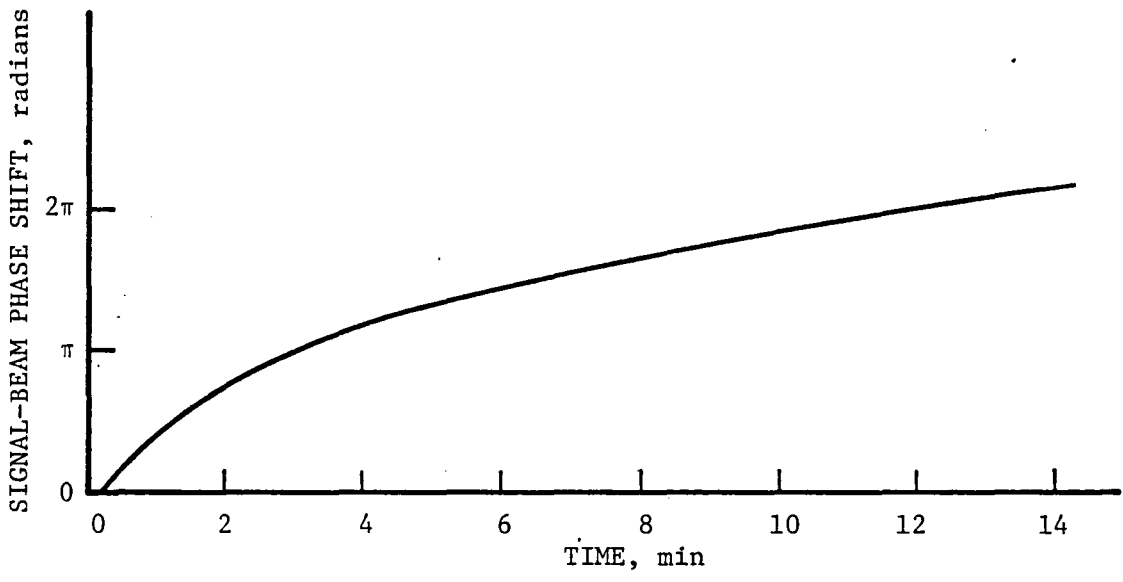


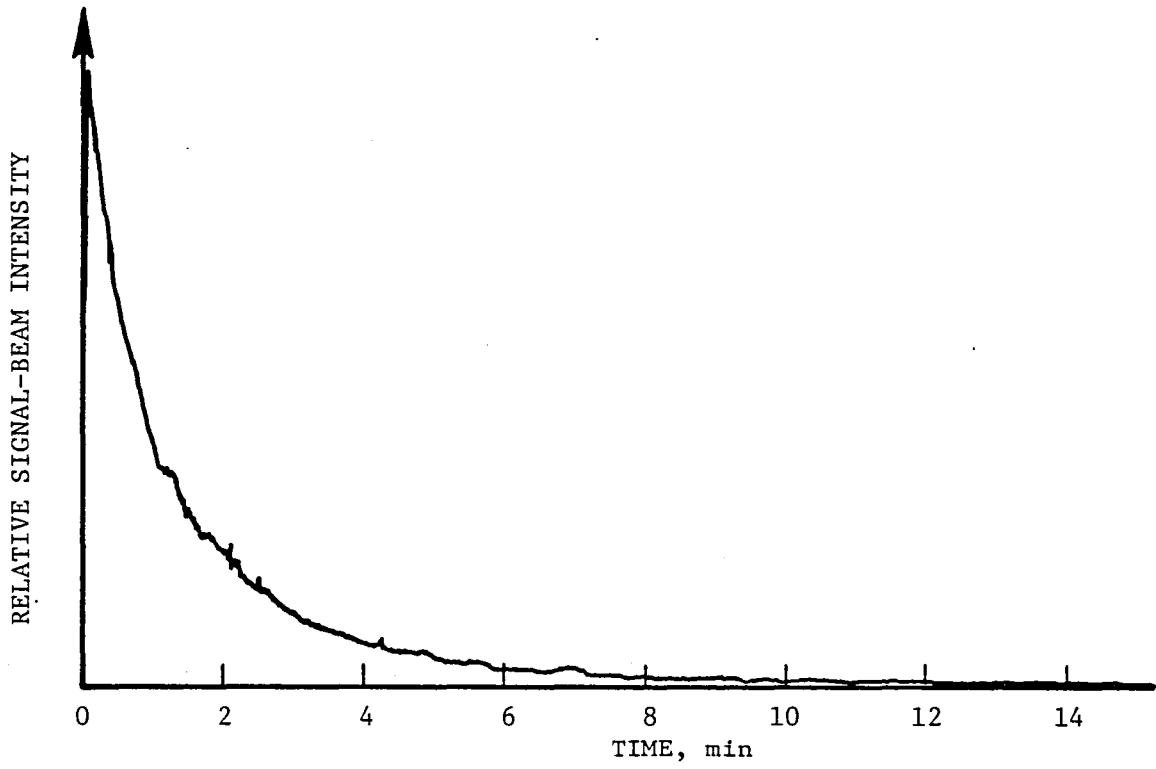
FIGURE IV-12. DAMPED OSCILLATORY SIGNAL-BEAM INTENSITY VS TIME CHARACTERISTICS EXHIBITED BY SAMPLE #162A.

The measurement of the optical phase of the beam undergoing subtraction was performed using the experimental set-up shown in Fig. III-3. A piezoelectrically positioned mirror was employed to keep a dark interference fringe centered on a detector as the fringe pattern attempted to move in response to changes in the subtracted-beam phase. The measured phase was therefore directly proportional to the voltage applied to the piezoelectric positioner. Calibration is performed by observing the voltage required to cause the detector to see a bright fringe ( $\pi$  phase shift).

The result of the experiment is shown in Fig. IV-13. Figure IV-13a shows the subtracted beam phase as a function of time on a linear scale calibrated in radians, while Fig. IV-13b shows the subtracted-beam intensity as a function of time on a relative linear scale. A total phase shift of approximately  $2\pi$  is observed over the recording interval. Theory predicts that a phase shift of this magnitude should result from two segregated  $\pi$  phase shifts that occur in the neighborhood of minima in the subtracted-beam intensity. In fact a rather continuous change in phase is observed. This is not surprising in view of the fact that the subtracted-beam intensity variation shows no apparent minima. We may speculate that the same physical mechanism that removes the oscillations in intensity also acts to smooth out sudden variations in phase. It is, however, somewhat reassuring to find that total phase changes as large as  $2\pi$  are observed at the same time that a significant measure of self-subtraction is observed, since this feature, at least, is compatible with the theoretical predictions of Sec. II.



(a) SIGNAL-BEAM PHASE SHIFT AS A FUNCTION OF RECORDING TIME



(b) RELATIVE SIGNAL-BEAM INTENSITY AS A FUNCTION OF RECORDING TIME

FIGURE IV-13. EXPERIMENTAL DETERMINATION OF SIGNAL-BEAM INTENSITY AND PHASE VARIATIONS DURING HOLOGRAM RECORDING.

## V. SUMMARY AND CONCLUSIONS

This report describes the results of an experimental and theoretical program to characterize and understand the holographic process termed self-subtraction. The program was very successful in its characterization objectives. A variety of  $\text{LiNbO}_3$  waveguide samples were evaluated with respect to self-subtraction parameters including (1) time constant for the development of a self-subtraction hologram, (2) minimum attainable null of the subtracted-beam intensity, as measured by the contrast ratio, (3) number of different self-subtraction holograms that can be recorded prior to the onset of material fatigue, and (4) stability of a self-subtraction hologram to long-term readout.

Sample #96 was characterized in depth regarding all four of these parameters. Other samples were tested until it was verified that they fell short of the performance of #96 in one or more areas. Sample #162A appeared comparable to #96, suggesting at least a limited degree of reproducibility, but it was not tested in depth.

The performance of sample #96 was very encouraging with regard to the possibility of someday using self-subtraction as a method for discriminating against slowly varying background information in an optical processor<sup>(2,3)</sup>. We found self-subtraction time constants in the vicinity of 150 sec, contrast ratios in excess of 40:1, stability of a self-subtraction hologram during readout for at least 7 h (the longest time examined), and reproducibility of the subtraction phenomena after five optical erasures in a single day (the largest number attempted). While these figures do not guarantee the ultimate utility of self subtraction as a "smart" optical-processing technique, we do regard their appearance in an initial program to be extremely promising.

On the negative side of the ledger, the present program had the dual objective of understanding the physical basis for self subtraction as well as characterizing the effect. It was hoped that this understanding would progress to the point where optimization of self-subtraction characteristics would be possible. With regard to achieving this objective the results of the program were, unfortunately, less than desired.

Theoretical calculations based on a simple but realistic photorefractive model showed that the beam undergoing self subtraction decreases in intensity in an oscillatory fashion. Experimentally, the decrease was more nearly exponential. Attempts to vary the photorefractive material properties by oxidizing and reducing heat treatments, and by the use of modified waveguide fabrication techniques, produced major changes in self-subtraction characteristics that could not be correlated with the theory. Even simple changes in the experimental geometry, such as changing the Bragg angle, produced unanticipated major changes in self subtraction.

Accordingly, we can not state that self subtraction is well understood as a result of the present work. While the effect has been demonstrated to a high level of satisfaction, our opinion is that improved understanding of the mechanism remains an important factor in any decision one might make as to the potential of self subtraction for optical processing. This understanding should come in part from experiments like those we have performed, with smaller perturbations of the crystals between measurements so that trends can be identified. In addition some type of measurement of the impurity state of the sample should be made with each run so that the effects of various heat treatment are known rather than inferred.

Theoretically, a more sophisticated photorefractive model than that employed here should be introduced. Attempts should be made to understand the quasiperiodic oscillations that sometimes occur in the signal-beam intensity in addition to the self-subtraction effect. Also, attempts to understand the physical basis for the observed sensitivity of self subtraction to the Bragg angle should be made.

With this type of effort, one might reasonably expect to optimize the self-subtraction effect for use in applications. As an additional benefit, considerable information will be added to the current understanding of photorefractivity, a holographic process that has relevance to many optical storage and processing systems, including some that function without the need or benefit of self subtraction.

## REFERENCES

1. K. Bromley, M. A. Monahan, J. F. Bryant, and B. J. Thompson, "Holographic Subtraction", *Appl. Opt.* 10 (1), 174-181 (1971).
2. D. W. Vahey, "'Smart' Remote Holographic Processor Based on the Materials Characteristics of  $\text{LiNbO}_3$ ", in Remote Sensing of Earth from Space: Role of "Smart Sensors", *Progress in Astronautics and Aeronautics*, 67, Roger Breckenridge, Ed., pp 352-366, American Institute of Aeronautics and Astronautics, 1979.
3. C. M. Verber, D. W. Vahey, R. P. Kenan, V. E. Wood, N. F. Hartman, and C. M. Chapman, "An Investigation for the Development of an Integrated-Optical Data Preprocessor", NASA Contractor Report 3151 prepared under contract NAS1-14655, Dec., 1978.
4. D. L. Staebler and J. J. Amodei, "Coupled-Wave Analysis of Holographic Storage in  $\text{LiNbO}_3$ ", *J. Appl. Phys.*, 43 (3), 1042-1049 (1972).
5. D. von der Linde and A. M. Glass, "Photorefractive Effects for Reversible Holographic Storage of Information", *Appl. Phys.*, 8, 85-100 (1975).
6. L. Young, W.K.Y. Wong, M.L.W. Thewalt, and W. D. Cornish, "Theory of Formation of Phase Holograms in  $\text{LiNbO}_3$ ", *Appl. Phys. Lett.*, 24 (6), 264-265 (1974).
7. D. M. Kim, R. R. Shah, T. A. Rabson, and F. K. Tittel, "Nonlinear Dynamic Theory for Photorefractive Phase Hologram Formation", *Appl. Phys. Lett.*, 28 (6), 338-340 (1976).
8. W. Phillips and D. L. Staebler, "Control of the  $\text{Fe}^{2+}$  Concentration in Iron-Doped Lithium Niobate", *J. Electron. Mater.*, 3 (2), 601-617 (1974).
9. H. Kurz, "Wavelength Dependence of the Photorefractive Process in  $\text{LiNbO}_3$ ", *Ferroelectrics*, 8 473-439 (1974).
10. D. von der Linde, O. F. Schirmer, and H. Kurz, "Intrinsic Photorefractive Effect of  $\text{LiNbO}_3$ ", *Appl. Phys.*, 15, 153-156 (1978).
11. A. M. Glass, D. von der Linde, and T. J. Negran, "High Voltage Bulk Photo-voltaic Effect and the Photorefractive Process in  $\text{LiNbO}_3$ ", *Appl. Phys. Lett.*, 25 (4), 233-235 (1974).
12. H. Kogelnik, "Coupled-Wave Theory for Thick Hologram Gratings", *Bell Syst. Tech. J.*, 48 (9), 2909-2947 (1969).
13. F. B. Hildebrand, Advanced Calculus for Applications, Chapter 4, pp 155-156 (Prentice-Hall, Englewood Cliffs, New Jersey, 1962).

14. R. Magnusson and T. K. Gaylord, "Use of Dynamic Theory to Describe Experimental Results from Volume Holography", J. Appl. Phys., 47 (1), 190-199 (1976).
15. M. G. Moharam, T. K. Gaylord, R. Magnusson and L. Young, "Holographic Grating Formation in Photorefractive Crystals with Arbitrary Electron Transport Lengths", J. Appl. Phys., 50 (9), 5642-5651 (1979).
16. L. Young, M. G. Moharam, F. El Guibaly, and E. Lun, "Hologram Writing in Lithium Niobate: Beam Coupling and the Transport Length in the Bulk Photo-voltaic Effect", J. Appl. Phys., 50 (6), 4201-4207 (1979).
17. V. Markov, S. Odulov, and M. Soskin, "Dynamic Holography and Optical Processing", Optics and Laser Technology, April 1979, pp 95-99.
18. N. Kukhtarev, V. Markov, and S. Odulov, "Transient Energy Transfer During Hologram Formation in LiNbO<sub>3</sub> in External Electric Field", Opt. Commun., 23 (3), 338-343 (1977).
19. A. Krumins and P. Günter, "Diffraction Efficiency and Energy Transfer During Hologram Formation in Reduced KNbO<sub>3</sub>", Appl. Phys., 19, 153-163 (1979).
20. L. Solymar, "A General Two Dimensional Theory for Volume Holograms", Appl. Phys. Lett., 31 (12), 820-822 (1977).
21. R. P. Kenan, "Theory of Crossed-Beam Diffraction Gratings", IEEE J. Quantum Electron., QE-14 (12), 924-930 (1978).
22. C. M. Verber, N. F. Hartman, and A. M. Glass, "Formation of Integrated Optics Components by Multiphoton Photorefractive Processes", Appl. Phys. Letts., 30 (6), 272-273 (1977).
23. W. K. Burns, P. H. Klein, E. J. West, and L. E. Plew, "Ti Diffusion in Ti:LiNbO<sub>3</sub> Planar and Channel Optical Waveguides", J. Appl. Phys., 50 (10), 6175-6182 (1979).
24. V. E. Wood, N. F. Hartman, and C. M. Verber, "Characteristics of Effused Slab Waveguides in LiNbO<sub>3</sub>", J. Appl. Phys., 45 (3), 1449-1451 (1974).
25. R. V. Schmidt, and H. Kogelnik, "Electro-Optically Switched Coupler with Stepped Delta-Beta Reversal Using Ti-Diffused LiNbO<sub>3</sub> Waveguides", Appl. Phys. Lett., 28 (9), 503-506 (1976).
26. S. K. Sheem, W. K. Burns, and A. F. Milton, "Leaky-Mode Propagation in Ti-Diffused LiNbO<sub>3</sub> and LiTaO<sub>3</sub> Waveguides", Opt. Letts., 3 (3), 76-78 (1978).
27. A. M. Glass, I. P. Kaminow, A. A. Ballman, and D. H. Olson, "Absorption Loss and Photorefractive Index Changes in Ti:LiNbO<sub>3</sub> Crystals and Waveguides", Appl. Opt., 19 (2), 276-281 (1980).

28. R. L. Holman, P. J. Cressman, and J. A. Anderson, "Processing and Properties of Diffused Lithium Niobate Planar Optical Waveguides", *Ferroelectrics*, 27 (1), 77-80 (1980).

1. Report No. NASA-CR-159336		2. Government Accession No.		3. Recipient's Catalog No.	
4. Title and Subtitle An Investigation of Self-Subtraction Holography in LiNbO <sub>3</sub>				5. Report Date July 21, 1980	
				6. Performing Organization Code	
7. Author(s) D. W. Vahey, R. P. Kenan, N. F. Hartman and R. C. Sherman				8. Performing Organization Report No.	
9. Performing Organization Name and Address Battelle Columbus Laboratories 505 King Avenue Columbus, Ohio 43201				10. Work Unit No.	
				11. Contract or Grant No. NAS1-15736	
12. Sponsoring Agency Name and Address National Aeronautics and Space Administration Washington, DC 20546				13. Type of Report and Period Covered Contractor Report	
				14. Sponsoring Agency Code	
15. Supplementary Notes Langley technical monitor: Marvin E. Beatty III Final Report					
16. Abstract This report describes the results of an investigation of self-subtraction holography in LiNbO <sub>3</sub> optical waveguides. Self subtraction describes the gradual transfer of energy from one optical beam to another that can occur when the two beams are used to record a hologram in LiNbO <sub>3</sub> . The effect is potentially useful in optical processors where the information signal is superimposed on a slowly varying and uninteresting background signal. Self subtraction affords the possibility of eliminating the background from the total signal received. The quality of self subtraction is inferred from measurements of the time required to form the hologram, the minimum beam intensity generated, the ability of the LiNbO <sub>3</sub> to form many successive holograms without fatigue, and the stability of the holograms during readout. In this program we tested in depth one sample having self-subtraction characteristics that were very promising: hologram-formation times were on the order of 150 sec, the null signal was less than 2.5% of the peak signal, and no fatigue nor instability was detected over the span of the experiments. Another sample, fabricated with, at most, slight modifications did not perform nearly as well. In all samples, attempts to improve self-subtraction characteristics by various thermal treatments had no effects or adverse effects, with one exception in which improvement was noted after a time delay of several days. A theory developed to describe self subtraction showed the observed decrease in beam intensity with time, but the shape of the predicted decay curve was oscillatory in contrast to the exponential-like decay observed. The theory was also inadequate to account for the experimental sensitivity of self subtraction to the Bragg angle of the hologram. We conclude that self subtraction is a viable method for optical processing systems requiring background discrimination. However, understanding the physical basis for the effect has only begun and further work of both an experimental and theoretical nature is required in order to optimize and control self subtraction for use in applications.					
17. Key Words (Suggested by Author(s)) Self-subtraction Holography LiNbO <sub>3</sub> Waveguides Integrated Optics Optical processing				18. Distribution Statement Background Discrimination Photorefractivity Fe:Oxidation-Reduction Unclassified - Unlimited	
19. Security Classif. (of this report) Unclassified		20. Security Classif. (of this page) Unclassified		21. No. of Pages 74	
22. Price*					

NASA Contractor Report 159336

Distribution List  
NASI-15736

No. of Copies

NASA Langley Research Center Hampton, VA 23665 Attn: Report and Manuscript Control Office, Mail Stop 180A	1
Technology Utilization Office, Mail Stop 139A	1
William M. Moore, Mail Stop 476	1
Dr. Roger A. Breckenridge, Mail Stop 473	1
Rodolfo Segura, Mail Stop 470	18
NASA Ames Research Center Moffett Field, CA 94035 Attn: Library, Mail Stop 202-3	1
NASA Dryden Flight Research Center P. O. Box 273 Edwards, CA 93523 Attn: Library	1
NASA Goddard Space Flight Center Greenbelt, MD 20771 Attn: Library	1
Gordon Chin, Code 693	1
NASA Lyndon B. Johnson Space Center 2101 Webster Seabrook Road Houston, TX 77058 Attn: JM6/Library	1
NASA Marshall Space Flight Center Marshall Space Flight Center, AL 35812 Attn: Library, AS61L	1
Jet Propulsion Laboratory 4800 Oak Grove Drive Pasadena, CA 91103 Attn: Library, Mail Code 111-113	1
Alan Johnston, Mail Code 198-336	1
NASA Lewis Research Center 21000 Brookpark Road Cleveland, OH 44135 Attn: Library, Mail Stop 60-3	1
NASA John F. Kennedy Space Center Kennedy Space Center, FL 32899 Attn: Library, NWSI-D	1
National Aeronautics and Space Administration Washington, DC 20546 Attn: RTE-6/Dr. Martin Sokolowski	3
RSI-5/Lee Holcomb	3

	<u>No. of Copies</u>
Prof. Joseph W. Goodman Dept. of Electrical Engineering Stanford University Stanford, CA 94305	1
Dr. Bob D. Guenther U. S. Army Research Office P. O. Box 12211 Attn: DRXRO-PH Research Triangle Park, NC 27709	1
Prof. Marion O. Hagler Dept. of Electrical Engineering Texas Tech University Lubbock, TX 79409	1
Mr. Alan Huang Information Systems Laboratory Stanford Electronic Laboratories Stanford, CA	1
Prof. Thomas F. Krile Dept. of Electrical Engineering Texas Tech University Lubbock, TX 79409	1
Dr. B. V. K. Vijaya Kumar Dept. of Electrical Engineering Carnegie-Mellon University Pittsburgh, PA 15213	1
Dr. John N. Lee Harry Diamond Laboratories Branch 13200 2800 Powder Mill Road Adelphi, MD 20783	1
Dr. Wai-Hon Lee Xerox Palo Alto Research Center 3333 Coyote Hill Road Palo Alto, CA 94304	1
Prof. Chen S. Tsai Dept. of Electrical Engineering Carnegie-Mellon University Pittsburgh, PA 15213	1
Dr. Carl M. Verber Battelle Columbus Laboratories 505 King Avenue Columbus, OH 43201	1

No. of Copies

Prof. Cardinal Warde  
Electrical Engineering and Computer Science  
Massachusetts Institute of Technology  
Cambridge, MA 02139

1

Dr. Carl C. Aleksoff  
ERIM  
P. O. Box 8618  
Ann Arbor, MI 48103

1

Mr. Thomas J. Bicknell  
Jet Propulsion Laboratory  
Building 183, Room #701  
4800 Oak Grove Drive  
Pasadena, CA 91103

1

Prof. Steven K. Case  
Dept. of Electrical Engineering  
University of Minnesota  
Minneapolis, MN 55455

1

Prof. Stuart A. Collins, Jr.  
Dept. of Electrical Engineering  
Ohio State University  
2015 Neil Avenue  
Columbus, OH 43210

1

Prof. James M. Florence  
Dept. of Electrical Engineering  
University of Texas  
Austin, TX 78712

1

Prof. Thomas K. Gaylord  
School of Electrical Engineering  
Georgia Institute of Technology  
Atlanta, GA 30332

1

Prof. Nicholas George  
Director, Institute of Optics  
University of Rochester  
Rochester, NY 14627

1

Dr. Mike Giles  
White Sands Missile Range  
Attn: STEWS-ID-T  
White Sands Missile Range, NM 88002

1

	<u>No. of Copies</u>
Dr. Robert D. Leighty U. S. Army Engineer Research Institute Topographic Labs Fort Belvoir, VA 22060	1
Prof. Emmett N. Leith Electrical and Computer Engineering Dept. University of Michigan Ann Arbor, MI 48109	1
Prof. Hau-Kuang Liu Dept. of Electrical Engineering University of Alabama University, AL 35486	1
Dr. Anthony Vander Lugt Harris Corporation P. O. Box 37 Melbourne, FL 32901	1
Prof. Robert J. Marks II Dept. of Electrical Engineering University of Washington Seattle, WA 98195	1
Mr. Michael A. Monahan Naval Ocean Systems Center NOSC Code 811 San Diego, CA 92152	1
Dr. John A. Neff Program Manager AFOSR/NE Bolling AFB, Washington, DC 20332	1
Prof. Thomas G. Newmann Dept. of Mathematics Texas Tech University Lubbock, TX 79409	1
Dr. William M. Portnoy Dept. of Electrical Engineering Texas Tech University Lubbock, TX	1
Prof. John F. Walkup Dept. of Electrical Engineering Texas Tech University Lubbock, TX 79409	1

No. of Copies

Mr. Harper Whitehouse  
Naval Ocean Systems Center  
NOSC Code 5303  
San Diego, CA 92152

1

Dr. Demetri Psaltis  
Dept. of Electrical Engineering  
Carnegie-Mellon University  
Pittsburgh, PA 15213

1

Prof. William T. Rhodes  
School of Electrical Engineering  
Georgia Institute of Technology  
Atlanta, GA 30332

1

Dr. William Sander  
U. S. Army Research Office  
P. O. Box 12211  
Attn: DRXRO-EL  
Research Triangle Park, NC 27709

1

Prof. Alexander A. Sawchuk  
Electrical Engineering Dept.  
Image Processing Institute  
University of Southern California  
Los Angeles, CA 90007

1

Dr. K. Terry Stalker  
Sandia National Laboratories  
Division 4426  
P. O. Box 5800  
Albuquerque, NM 87185

1

Dr. William Stoner  
Science Applications, Inc.  
3 Preston Court  
Bedford, MA 01730

1

Prof. Armand R. Tanguay, Jr.  
Depts. of Electrical Engineering and Materials Science  
University of Southern California  
Los Angeles, CA 90007

1

NASA Scientific and Technical Information Facility  
6571 Elkridge Landing Road  
Linthicum Heights, MD 21090

25 plus  
original

**End of Document**